European Journal of Medicinal Chemistry 211 (2021) 113117

Contents lists available at ScienceDirect

European Journal of Medicinal Chemistry

journal homepage: http://www.elsevier.com/locate/ejmech

Discovery of novel 2-aryl-3-sulfonamido-pyridines (HoAns) as microtubule polymerization inhibitors with potent antitumor activities

Heping Zhu [a], Shilong Ying [b], Bingluo Zhou [b], Xiao Liang [b], Quan He [a], Ping Song [b], Xinyang Hu [b], Keqiang Shi [b], Mingteng Xiong [a], Hongchuan Jin [b, **], Yuanjiang Pan [a, *]

[a] Department of Chemistry, Zhejiang University, Hangzhou, 310027, PR China
[b] Laboratory of Cancer Biology, Key Lab of Biotherapy in Zhejiang, Sir Run Run Shaw Hospital, Medical School of Zhejiang University, Hangzhou, 310020, PR China

ARTICLE INFO

Article history:
Received 8 October 2020
Received in revised form
14 December 2020
Accepted 16 December 2020
Available online 25 December 2020

Keywords:
2-Aryl-3-sulfonamido-pyridines
Synthesis
Tubulin polymerization
Microtubule-targeting agents
Antitumor activity

ABSTRACT

Microtubules play a vital role in cell mitosis. Drugs targeting taxol or vinca binding site of tubulin have been proved an effective way to against cancer. However, drug resistance and cancer recurrence are inevitable, there is an urgent need to search for new microtubule-targeting agents (MTAs). In our study, a series of novel 2-aryl-3-sulfonamido-pyridines (**HoAns**) had been designed, synthesized, and evaluated for their antiproliferative activities *in vitro* and *in vivo*. Among them, compound **HoAn32** exhibited the most potent activity with IC_{50} values ranging from 0.170 to 1.193 μM in a panel of cancer cell lines. Mechanism studies indicated that compound **HoAn32** bound to the colchicine site of β-tubulin, resulting in colony formation inhibition, G2/M phase cell cycle arrest, cell apoptosis as well as increased the generation of ROS in both RKO and SW620 cells. In addition, compound **HoAn32** showed potent anti-vascular activity *in vitro*. Furthermore, compound **HoAn32** also exhibited outstanding antitumor activity in SW620 xenograft tumor models without observable toxic effects, which was more potent than that of **ABT-751**. In conclusion, our findings suggest that compound **HoAn32** may be a promising microtubule destabilizing agent and deserves for further development in cancer therapy.

1. Introduction

Microtubules are ubiquitous in eukaryotic cells with hollow tubular structure, which mainly consist of α- and β-tubulin heterodimers [1]. The dynamic properties of continuous polymerization and depolymerization of the microtubule are the basis for its multiple functions, including maintaining cell morphology, mediating cell signal transduction, participating cell mitosis, cytoplasmic transportation and organelle localization, etc. [2–5] Comparing with normal cells, cell mitosis in tumor cells is abnormally frequent, and microtubules play an important role in it [6]. Inhibiting or promoting tubulin polymerization could block tumor cell mitosis, induce apoptosis and promote cell death eventually [7]. Microtubule-targeting agents (MTAs) can be divided into two categories, one is microtubule stabilizing agent targeting the taxol binding site [8] or laulimalide binding site [9], and the other is microtubule destabilizing agent, which specially targeting the colchicine binding site [10] or vinca binding site [11]. Classic MTAs such as paclitaxel, docetaxel, vincristine, vinorelbine and so forth have been used in clinic for a long history. Although these drugs exhibited strong antitumor effects, some limitations such as severe side effects, drug resistance and cancer recurrence must be noted [12,13]. Lots of efforts had been made in the process to discover small molecular colchicine site binding agents [14], and some excellent agents such as Combretastatin A-4 phosphate (**CA4P**)

Abbreviations: BSA, bovine serum albumin; DAPI, 4,6-diamidino-2-phenylindole; DCFH-DA, 2′, 7′-dichlorofluorescein diacetate; DMAP, 4-dimethylaminopyridine; DMSO, dimethyl sulfoxide; DTT, dithiothreitol; EA, ethyl acetate; EBI, *N,N′*-ethylene-bis(iodoacetamide); H&E, Hematoxylin/ eosin; MTAs, Microtubule-targeting agents; MTS, 3-(4,5-dimethylthiazol-2-yl)-5-(3-carboxymethoxyphenyl)-2-(4-sulfophenyl)-2H-tetrazolium; PBS, phosphate buffered saline; $Pd(PPh_3)_4$, Terakis(triphenylphosphine)palladium(0); PE, petroleum ether; PI, propidium iodide; ROS, reactive oxidative stress; SDS, sodium dodecyl sulfate; TEA, triethylamine; THF, tetrahydrofuran; TLC, thin-layer chromatography; Tris, 2-amino-2-hydroxymethyl-1,3-propandiol.

* Corresponding author.
** Corresponding author.
E-mail addresses: jinhc@zju.edu.cn (H. Jin), panyuanjiang@zju.edu.cn (Y. Pan).

https://doi.org/10.1016/j.ejmech.2020.113117
0223-5234/

[15], **ABT-751** [16], Plinabulin (**NPI-2358**) [17] and so forth had already been successfully entering clinical trials. Despite the investigations of these agents as a single drug or in combination with other drugs in cancer patients, there is still a long way to go to be finally marketed. For example, **ABT-751** is a classic sulfonamide tubulin polymerization inhibitor, which has more than 10 clinical research projects (see https://clinicaltrials.gov/) up to now, however, there are few reports of its further clinical progress, which may be associated with its low objective response rate in cancer patients [18–20]. Considering the far unmet needs for clinical oncology patients, searching for new colchicine site binding agents is of great significance.

In this work, the strategy of pharmacophore fusion was applied in our design. On the one hand, the biaryl moieties have frequently been observed in the naturally occurred products with potential antitubulin activity (e.g. Honokiol [21], Fig. 1) as well as in the synthetic antitubulin agents (e.g. **compound 4v** [22] and **compound 21** [23], Fig. 1). On the other hand, some agents containing arylsulfonamide motif had been proved as MTAs with strong anticancer activities such as **T138067** [24], **ABT-751** [16] as well as **ELR510444** [25] (Fig. 1), etc. We speculated that the fusion of these two pharmacophores may produce a new structure type of antitubulin agents. In view of this, we merged these two pharmacophores and designed a series of novel 2-aryl-3-sulfonamido-pyridines, which we named **HoAns** uniformly (Fig. 1). Herein, we reported the discovery of these novel derivatives as potent microtubule polymerization inhibitor targeting the colchicine binding site and exploring their antitumor activities *in vitro* and *in vivo*.

2. Results and discussion

2.1. Chemistry

In order to obtain the newly designed 2-aryl-3-sulfonamido-pyridines (**HoAns**), several classic organic reactions were applied. Compounds **HoAn1**-**HoAn31** were designed and synthesized firstly. The synthetic routes of **HoAn1** to **HoAn31** were shown in Schemes 1 and 2. Nucleophilic substitution reaction between commercially available 2-bromopyridin-3-amine (**1**) and 4-methoxybenzenesulfonyl chloride in alkaline condition with DMAP catalysis produced intermediate **2**. Then, Suzuki coupling of intermediate **2** with phenylboronic acid substituted with hydroxyl groups in different positions by using cheap metal catalyst $Pd(PPh_3)_4$ under K_2CO_3 condition afforded the desired products **HoAn11**-**HoAn13**. When we prepared the intermediate **2u**-**2w**, the Suzuki coupling reaction would take place with a moderate yield when the reaction temperature turned up to 120 °C and the solvent replaced by 1,4-dioxane/H_2O between intermediate **1** and boric acid containing N heterocyclic ring. Subsequently, the final products **HoAn25**-**HoAn27** were obtained via the reaction between intermediate **2u**-**2w** and 4-methoxybenzenesulfonyl chloride. Starting with intermediate **1**, Suzuki coupling with different substituted phenylboronic acid could get intermediate **2a**-**2t**. Then, the final products **HoAn1**-**HoAn10**, **HoAn14**-**HoAn16**, **HoAn18** and **HoAn20**-**HoAn24** obtained by intermediate **2a**-**2s** reacted with 4-methoxybenzenesulfonyl chloride, the reaction condition was similar to the way to produce intermediate **2**. For the synthesis of **HoAn28**-**HoAn31**, intermediate **2d-2f** or **2q** reacted with 4-methoxybenzenesulfonyl chloride in another condition, which used TEA instead of DMAP as the catalyst and the dosage of TEA was elevated to three times. The target products **HoAn17** and **HoAn19** could be obtained through reduction reaction, which via **HoAn16** or **HoAn18** reacted in NH_4Cl condition and catalysis with iron power directly.

For the compounds designed in the second step, the synthetic routes were showed in Scheme 3. The desire products **HoAn32**-**HoAn40** could be obtained via the reaction between intermediate **2t** and various substituted benzenesulfonyl chloride or naphthalenesulfonyl chloride with a synthetic condition similar to the synthesis of intermediate **2**.

2.2. Biology

2.2.1. In vitro human cancer cell line growth inhibition assay

The *in vitro* antiproliferative efficacy of compounds **HoAn1**-**HoAn31** were first evaluated towards three different kinds of human cancer lines, including MCF-7 (human breast cancer cell), SK-HEP-1 (human hepatoma cells) and RKO (human colon adenocarcinoma cell) by MTS assay and compared with Honokiol as well as **ABT-751**. As shown in Fig. 2, among all the 31 newly designed **HoAns**, four of which including **HoAn15** (R_1 = 4-CF_3), **HoAn16** (R_1 = 4-NO_2), **HoAn20** (R_1 = 4-CN) and **HoAn24** (R_1 = H) displayed better inhibitory activities against these three cancer cell lines. In detail, the cell viability of MCF-7 cells after treatment with these four compounds and **ABT-751** for 72 h at 10 μM was 63.4%, 58.90%, 54.95%, 65.68% and 40.00%, respectively. However, the MCF-7 cells seem not sensitive to the other twenty-seven **HoAns** (**HoAn1**-**HoAn14**, **HoAn17**-**HoAn19**, **HoAn21**-**HoAn23** and **HoAn25**-**HoAn31**) as well as Honokiol, the cell viabilities of which were all exceeded 70% (Fig. 2). The similar results also happened in SK-HEP-1 cells. As illustrated in Fig. 2, after treatment with these compounds for 72 h at 10 μM, only **HoAn15**, **HoAn16**, **HoAn20**, **HoAn24**

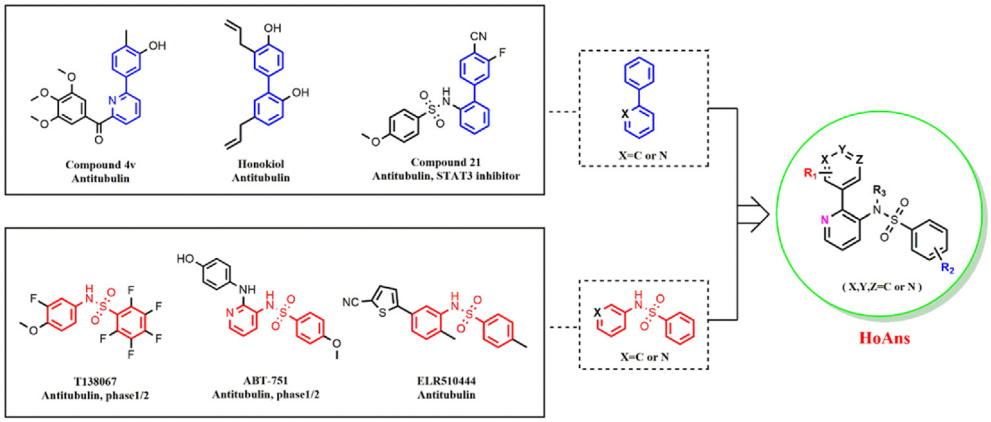

Fig. 1. Design strategy of novel 2-aryl-3-sulfonamido-pyridines (**HoAns**).

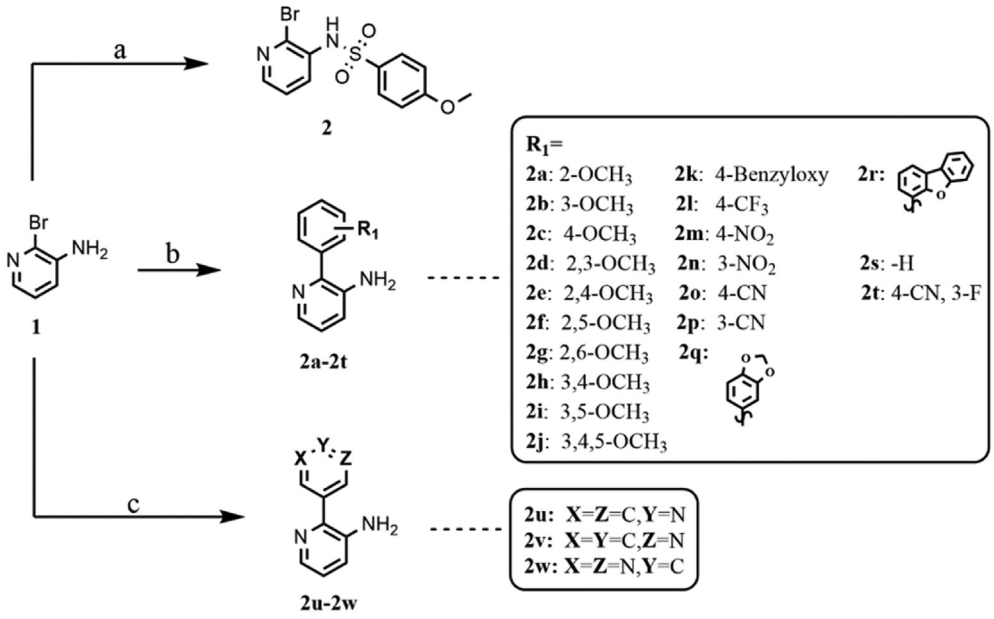

Scheme 1. Synthetic Route of Key Intermediates 2 and 2a-2w[a].
[a]**Reagents and conditions**: a). 4-methoxybenzenesulfonyl chloride (1.2 eq), DMAP (0.5 eq), pyridine, CH_2Cl_2, 60–70 °C, reflux, 8–12 h; b). various substituted phenylboronic acids (1 eq), $Pd(PPh_3)_4$ (0.05 eq), K_2CO_3 (3 eq), toluene/H_2O = 2/1 (v/v), N_2, 80–85 °C, reflux, 8–10 h; c). various pyridylboronic acids (1 eq) or 5-pyrimidinylboronic acid (1 eq), $Pd(PPh_3)_4$ (0.05 eq), K_2CO_3 (3 eq), 1,4-dioxane/H_2O = 2/1 (v/v), N_2, 120 °C, reflux, 12 h.

and **ABT-751** showed preferable inhibitory activities, the cell viabilities of SK-HEP-1 were 64.00%, 40.76%, 12.44%, 68.04% and 5.97%, respectively. For RKO cells, after incubated with these compounds under the same condition, **HoAn15**, **HoAn16**, **HoAn20**, **HoAn24** and **ABT-751** still showing the best antiproliferative efficacy, the cell viabilities were all below 40% and the values were 33.08%, 21.80%, 13.44%, 35.10% and 16.30%, respectively. Meanwhile, several **HoAns** such as **HoAn18** (R_1 = 3-NO_2), **HoAn21** (R_1 = 3-CN) and **HoAn25** (**X** = **Z** = C, **Y**=N) as well as Honokiol also exhibited inhibitory efficacy, the cell viability of which was 60.62%, 51.79%, 58.57% and 49.67%, respectively (Fig. 2). On the basis of these results, we chose **HoAn15**, **HoAn16**, **HoAn20** and **HoAn24** as representative compounds for further antiproliferative efficacy screening.

Subsequently, the IC_{50} values of compounds **HoAn15**, **HoAn16**, **HoAn20** and **HoAn24** were measured by MTS assay towards ten different kinds of human cancer cell lines, including two human liver cancer cell lines (PLC/PRF/5 and HCC-LM3), two human breast cancer cell lines (BT474 and SK-BR-3), three human colon cancer cell lines (RKO, SW620 and SW480), two lung cancer cell lines (A549 and H460) and one human pancreatic cancer cell line (PANC-1) in comparison with **ABT-751**. As shown in Table 1, among these representative **HoAns**, compound **HoAn20** showed the strongest and broad-spectrum antiproliferative activities against these ten cancer cell lines, the IC_{50} values of which were ranged from 0.204 μM to 2.457 μM. We observed that RKO, SW620 and SW480 cells were more sensitive to **HoAn20** than other types of cancer cells, the IC_{50} values of which were 0.259 μM, 0.607 μM and 0.204 μM, respectively, and the efficacy was better than **ABT-751** (IC_{50} = 0.633 μM, 2.787 μM and 3.421 μM, respectively). Compound **HoAn15** showed less potent against these cell lines, the IC_{50} values were all exceeded 10 μM apart from colon cancer cell lines, the IC_{50} values were 4.048 μM, 6.818 μM and 9.214 μM, respectively after acting on RKO, SW620 and SW480 cells for 72 h. Likewise, compound **HoAn24** was also exhibited antiproliferative activities only in human colon cancer cell lines, the IC_{50} values were 4.324 μM and 7.886 μM when against RKO and SW620 cells, while the IC_{50} values against other cell lines were all more than 10 μM. Additionally, except BT474, A549 and H460 cells (IC_{50} > 10 μM), other seven cancer cell lines were sensitive to **HoAn16**, the IC_{50} values of which were ranged from 1.403 μM to 7.589 μM. Notably, although **HoAn20** showed better antiproliferative activities in three different human colon cancer cell lines and BT474 (IC_{50} = 1.336 μM) as well as H460 (IC_{50} = 1.496 μM) than **ABT-751** (IC_{50} = 8.390 μM for BT474 cells and IC_{50} = 2.036 μM for H460 cells), the efficacy of **HoAn20** against other cancer cell lines, including PLC/PRF/5, HCC-LM3, SK-BR-3, A549 and PANC-1 was inferior to **ABT-751** under the same conditions (Table 1). Therefore, the structural modification of **HoAn20** was carried out afterwards.

Previously, Meanwell NA [26] reviewed the functions and applications of fluorine and fluorinated motifs as bioisosteres in drug design. Inspired by his article, we introduced a fluorine atom adjacent to the cyano group and made some modifications on the benzenesulfonamide part, and finally designed nine new **HoAns** (**HoAn32**-**HoAn40**) to compare with **HoAn20**. The antiproliferative activities of these new compounds against three different cancer cell lines, including HCC-LM3, RKO and PANC-1 were evaluated initially. As shown in Table 2, the antiproliferative efficacy against RKO and PANC-1 cells was both improved after incubated with **HoAn32** (R_2 = 4″-OCH_3) for 72 h, and the IC_{50} values of which were 0.170 μM and 0.729 μM, respectively, and the efficacy against HCC-LM3 of **HoAn32** (IC_{50} = 0.963 μM) was not lost much. To our surprise, modifications on the benzenesulfonamide part were inoperative for improving antiproliferative efficacy, but reduced the efficacy. The efficacy against RKO cells was about 35-fold loss for **HoAn33** (R_2 = 4″-CH_3) and 11-fold loss for **HoAn38** (R_2 = 2″-naphthalene), and the efficacy against HCC-LM3 cells was about 12-fold loss for **HoAn38** when compared with **HoAn20**. For the rest compounds, including **HoAn34** (R_2 = 4″-Cl), **HoAn35** (R_2 = 4″-Br), **HoAn36** (R_2 = 4″-CF_3), **HoAn37** (R_2 = H), **HoAn39** (R_2 = 4″-OCF_3) and **HoAn40** (R_2 = 3″, 4″-OCH_3), the IC_{50} values of which against these three cancer cell lines were all over 10 μM. Next, we tested the antiproliferative efficacy of **HoAn32** in other five human cancer cell lines. The results indicated that, comparing with **HoAn20**, compound **HoAn32** maintained or even improved the antiproliferative activities, the IC_{50} values of which against SK-BR-3,

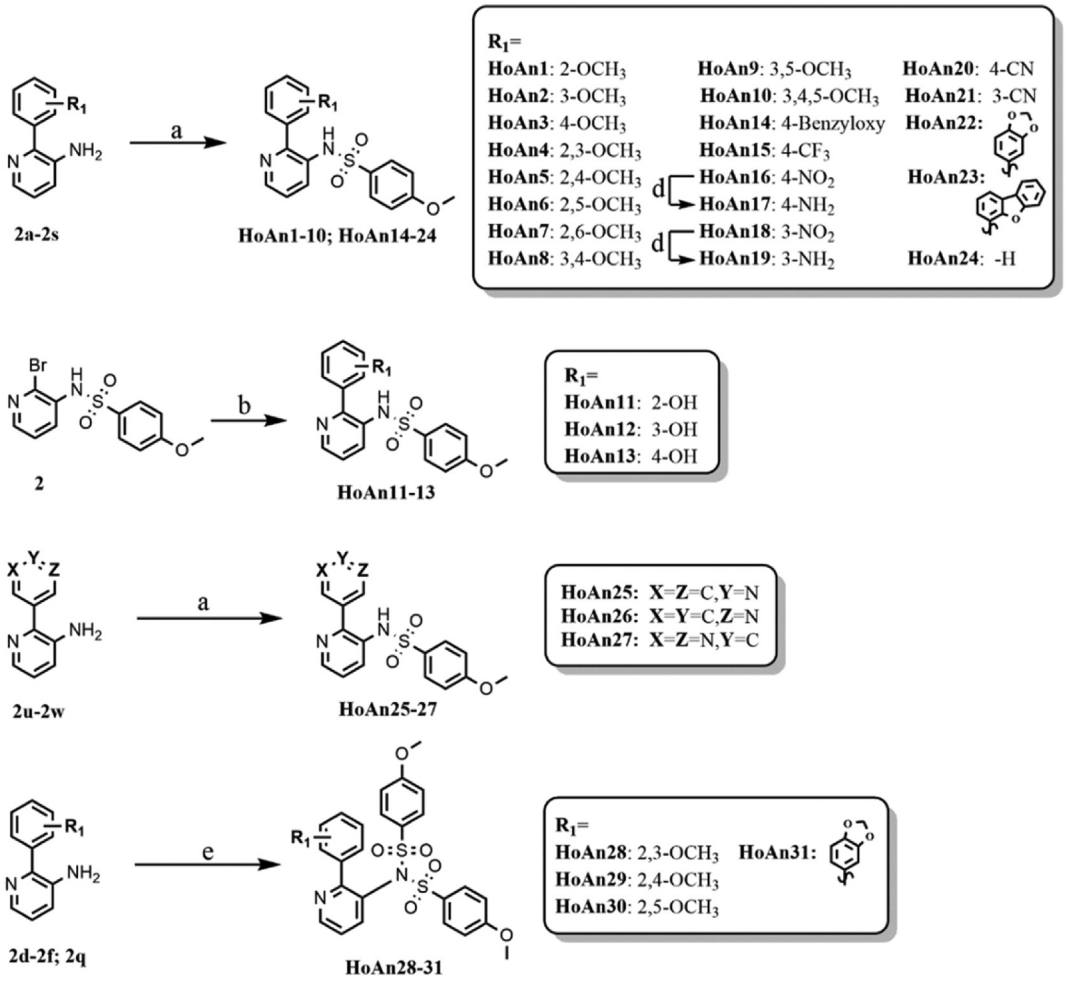

Scheme 2. Synthetic Route of Target Compounds HoAn1-HoAn31[a].
[a]**Reagents and conditions**: The synthetic conditions of routes **a** and **b** were same as the routes described in Scheme 1; d). iron powder (10 eq), NH_4Cl (3 eq), ethanol/H_2O = 2/1 (v/v), 95 °C, reflux, 1–3 h; e). 4-methoxybenzenesulfonyl chloride (3 eq), TEA (5 eq), CH_2Cl_2, 60–70 °C, reflux, 10–12 h.

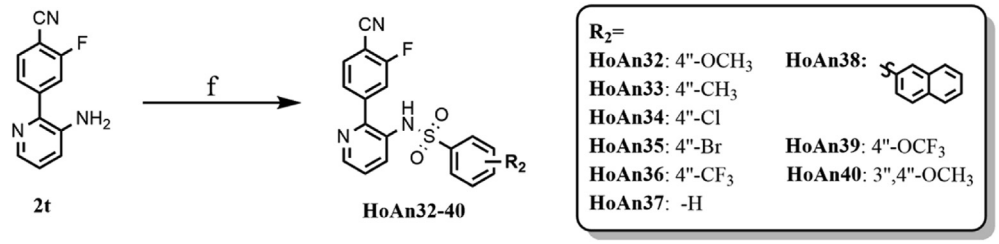

Scheme 3. Synthetic Route of Target Compounds HoAn32-HoAn40[a].
[a]**Reagents and conditions**: f). various substituted benzenesulfonyl chloride (1.2 eq) or 2-naphthalenesulfonyl chloride (1.2 eq), DMAP (0.5 eq), pyridine, CH_2Cl_2, 60–70 °C, reflux, 10–12 h.

BT474, SW620, SW480 and SGC-7901 cells were 0.431 μM, 1.193 μM, 0.673 μM, 0.338 μM and 0.617 μM, respectively (Table 2). The results also indicated that compound **HoAn32** possesses better antiproliferative activities in these cell lines except HCC-LM3 and SK-BR-3 cell lines than **ABT-751** (Table 2). The summarized SARs of the newly synthesized compounds was illustrated in Fig. 3.

Furthermore, the long-term inhibitory effect of **HoAn32** treatment was performed by colony-formation assay. After treatment with **HoAn32** or **ABT-751** at different concentrations for 24 h in RKO and SW620 cells, the cell colonies were continuing to cultivate for another 10 days with fresh culture medium until staining with crystal violet and photographed. The results showed that **HoAn32** treatment produced a stronger inhibitory effect on both RKO (Fig. 4A) and SW620 (Fig. 4B) cells growth in a dose-dependent manner (from 0.125 μM to 1 μM) when compared with the negative control. At the same concentration (1 μM), the inhibitory effect against both cell lines of **HoAn32** was better than **ABT-751**.

Based on the *in vitro* antiproliferative activity results, undoubtedly, we selected compound **HoAn32** for further anticancer mechanism studies.

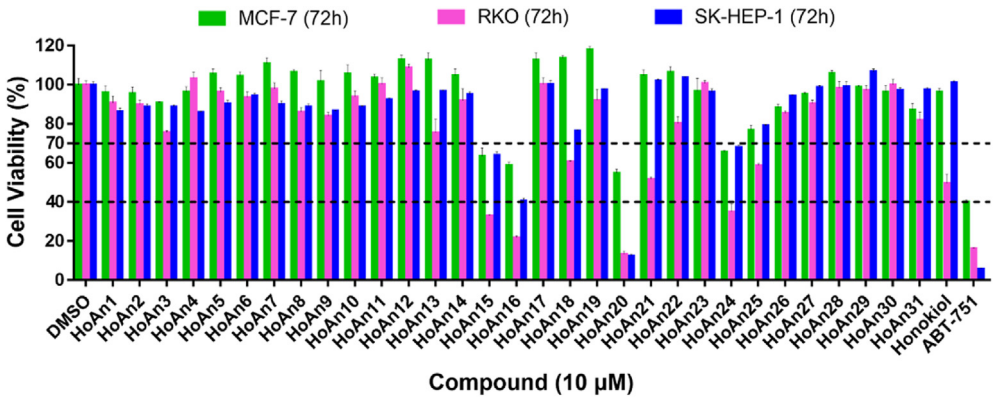

Fig. 2. In Vitro Antiproliferative Activities of Compounds **HoAn1**-**HoAn31**, **Honokiol** and **ABT-751** against MCF-7, SK-HEP-1 and RKO cell. The cells were treated with **HoAn1**-**HoAn31**, **Honokiol** and **ABT-751** at 10 μM for 72 h, and the cell viability was finally determined by MTS assay.

Table 1
In Vitro Antiproliferative Activities of Representative Compounds **HoAn15**, **HoAn16**, **HoAn20** and **HoAn24** as well as **ABT-751** against Different Kinds of Cancer Cell Lines[a].

Comp.		HoAn15	HoAn16	HoAn20	HoAn24	ABT-751
R_1		4-CF_3	4-NO_2	4-CN	-H	
Cell Types	*Cell Lines*	IC_{50} (μM)[b]				
Liver cancer	PLC/PRF/5	>10	5.296 ± 0.151	**0.816 ± 0.024**	>10	0.792 ± 0.019
	HCC-LM3	>10	7.598 ± 0.186	**0.747 ± 0.018**	>10	0.671 ± 0.021
Breast cancer	BT474	>10	>10	**1.336 ± 0.243**	>10	8.390 ± 1.028
	SK-BR-3	>10	6.307 ± 0.088	**0.746 ± 0.066**	>10	0.143 ± 0.015
Colon cancer	RKO	4.048 ± 0.242	1.403 ± 0.042	**0.259 ± 0.013**	4.324 ± 0.507	0.633 ± 0.011
	SW620	6.818 ± 0.573	3.625 ± 0.443	**0.607 ± 0.031**	7.886 ± 0.295	2.787 ± 0.072
	SW480	9.214 ± 1.189	3.855 ± 0.289	**0.204 ± 0.019**	>10	3.421 ± 0.141
Lung cancer	A549	>10	>10	**2.457 ± 0.162**	>10	1.376 ± 0.147
	H460	>10	>10	**1.496 ± 0.189**	>10	2.036 ± 0.282
Pancreatic cancer	PANC-1	>10	7.192 ± 0.102	**1.089 ± 0.146**	>10	0.837 ± 0.016

[a] Cells were treated with different concentrations of the compounds for 72 h. Cell viability was measured by an MTS assay.
[b] IC_{50} values are indicated as the mean ± SD (standard deviation) and all the experiments performed at least three times.

Table 2
In vitro antiproliferative activities of compounds **HoAn32**–**HoAn40** and **ABT-751** against different kinds of cancer cell Lines[a].

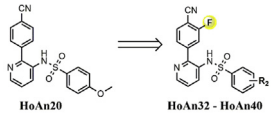

Comp.	R_2	IC_{50} (μM)[b]							
		HCC-LM3	RKO	PANC-1	SK-BR-3	BT474	SW620	SW480	SGC-7901
HoAn32	4′′-OCH_3	**0.963 ± 0.157**	**0.170 ± 0.012**	**0.729 ± 0.037**	**0.431 ± 0.031**	**1.193 ± 0.146**	**0.673 ± 0.015**	**0.338 ± 0.018**	**0.617 ± 0.035**
HoAn33	4′′-CH_3	>10	9.207 ± 0.699	>10	N.D[c]	N.D	N.D	N.D	N.D
HoAn34	4′′-Cl	>10	>10	>10	N.D	N.D	N.D	N.D	N.D
HoAn35	4′′-Br	>10	>10	>10	N.D	N.D	N.D	N.D	N.D
HoAn36	4′′-CF_3	>10	>10	>10	N.D	N.D	N.D	N.D	N.D
HoAn37	-H	>10	>10	>10	N.D	N.D	N.D	N.D	N.D
HoAn38		8.865 ± 0.514	2.922 ± 0.256	10.02 ± 0.852	N.D	N.D	N.D	N.D	N.D
HoAn39	4′′-OCF_3	>10	>10	>10	N.D	N.D	N.D	N.D	N.D
HoAn40	3′′,4′′-OCH_3	>10	>10	>10	N.D	N.D	N.D	N.D	N.D
ABT-751		0.671 ± 0.021	0.633 ± 0.011	0.837 ± 0.016	0.143 ± 0.015	8.390 ± 1.028	2.787 ± 0.072	3.421 ± 0.141	0.738 ± 0.045

[a] Cells were treated with different concentrations of the compounds for 72 h. Cell viability was measured by MTS assay.
[b] IC_{50} values are indicated as the mean ± SD (standard deviation) and all the experiments performed at least three times.
[c] N.D means not detected.

2.2.2. Compound HoAn32 inhibited microtubule assembly and colchicine binding effects

The *in vitro* tubulin polymerization assay was performed to determine whether the broad-spectrum antiproliferative activities of **HoAn32** was caused by interfering microtubule systems or not. As shown in Fig. 5, the tubulin polymerization was almost

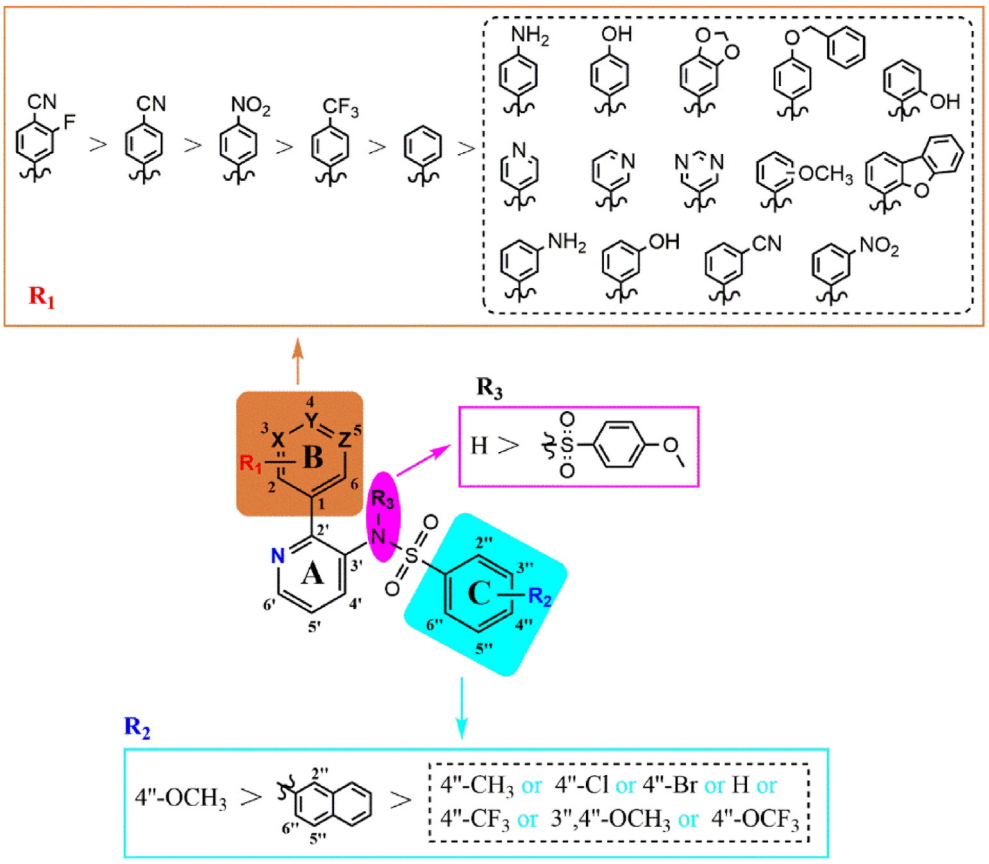

Fig. 3. SARs summary of the newly synthesized compounds.

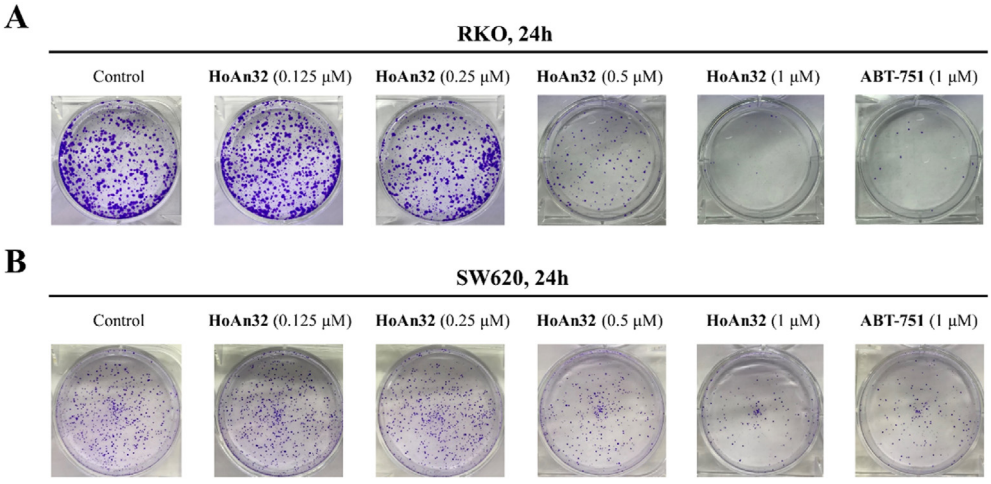

Fig. 4. Effect of compound **HoAn32** on RKO cells (A) and SW620 cells (B) colony formation. Cells were incubated with **HoAn32** (0.125, 0.25, 0.5 and 1 μM) and **ABT-751** (1 μM) for 24 h and continue to grow for another 10 days with fresh culture medium. Visualized colonies were photographed.

completely inhibited after pre-incubated with **HoAn32** at 10 μM concentration, and the inhibition efficacy was similar with **ABT-751**, while the positive control paclitaxel strongly and consistently promoted tubulin polymerization under the same conditions. We next observed the effect of **HoAn32** on the microtubule network by immunofluorescence via fluorescence microscopy. As illustrated in Fig. 6, the microtubule morphology in RKO cells was incompact and fragmentation after treatment with **HoAn32** at 0.5 μM for 24 h, while in the higher concentration group (**HoAn32**, 1 μM), the cell morphology changed more obvious, the shapes of which gradually turned to round from fusiform, and the phenomenon was also observed in **ABT-751** (1 μM) administration group. Meanwhile, paclitaxel (1 μM) displayed an opposite way of disturbing the microtubule network, which promoted tubulin polymerization and made microtubule morphology more densification and aggregation (Fig. 6).

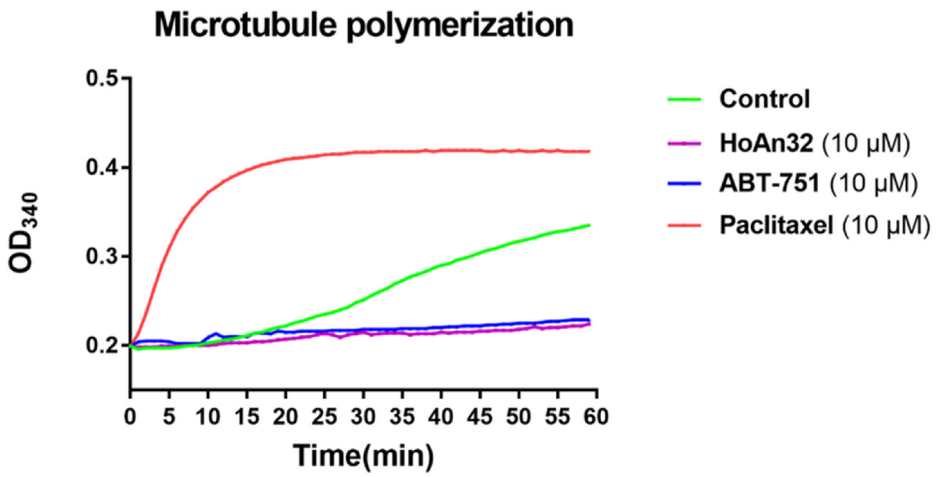

Fig. 5. Effect of compound **HoAn32** on microtubule polymerization *in vitro*. The microtubule polymerization experiments were performed with a commercial kit (#BK004P, Cytoskeleton). In brief, tubulin (4 mg/mL) was exposed to vehicle control and 10 μM of the compounds (**HoAn32**, **ABT-751** and paclitaxel), and then the absorbance at 340 nm was monitored at 37 °C every minute for 60 min by microplate reader.

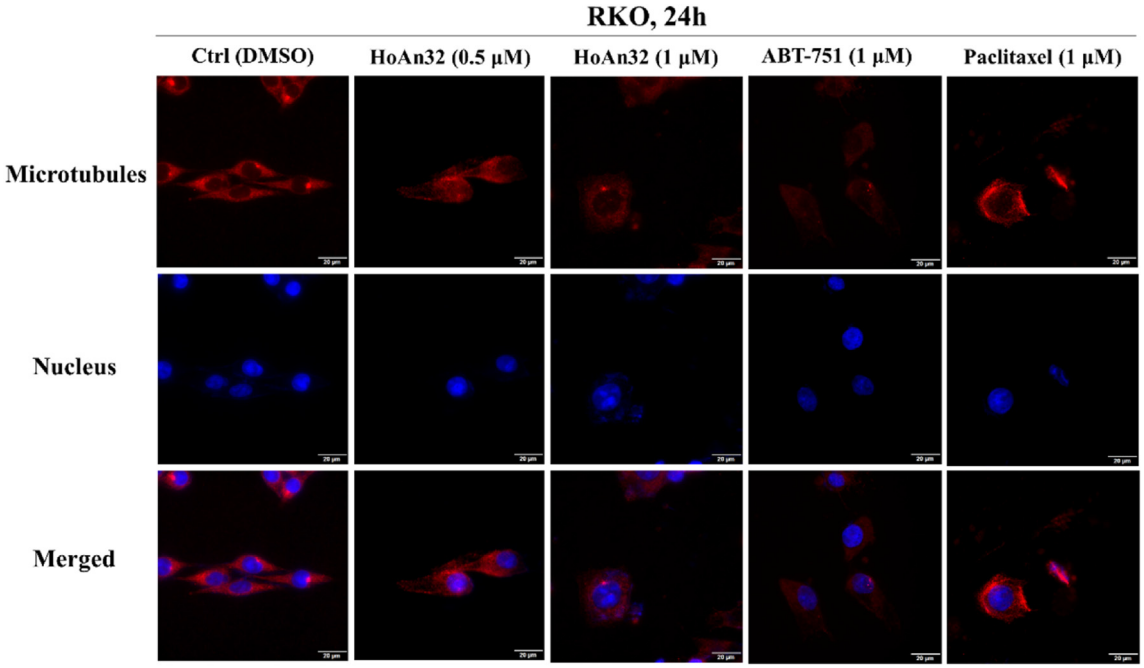

Fig. 6. Immunofluorescence assay analysis of the effect of compound **HoAn32** on the cellular microtubule network. RKO cells were treated with DMSO, **HoAn32** (0.5 μM and 1 μM), **ABT-751** (1 μM) and Paclitaxel (1 μM) for 24 h, and then the cells were fixed and stained with the anti-β-tubulin antibody (red), Alexa Fluor Plus 594 dye and nucleuses were stained with DAPI (blue). Images were performed by using Olympus BX53 microscope (Tokyo, Japan). (For interpretation of the references to colour in this figure legend, the reader is referred to the Web version of this article.)

EBI (*N*,*N*′-ethylene-bis(iodoacetamide)) is an alkylating agent, which can alkylate the colchicine site of β-tubulin in Cys-239 and Cys-354 sites to form β-tubulin-EBI adducts [27]. To find out the detailed mechanism of **HoAn32** acting on tubulin polymerization, we next carried out the EBI competition assay to determine whether it could bind to the colchicine site of β-tubulin or not. As shown in Fig. 7A, the results revealed that **HoAn32** indeed could compete with EBI (100 μM) binding to the colchicine site in β-tubulin with a dose dependent manner (from 10 μM to 40 μM) in SW620 cells, and the phenomenon was also occurred in **ABT-751** (20 and 40 μM) treatment group, which had been proved binding with colchicine site of tubulin previously [28]. The results indicated that **HoAn32** bind to the colchicine site of β-tubulin.

2.2.3. Molecular docking studies of HoAn32 with tubulin

Based on the above results, to further gain insight on the possible binding mode of **HoAn32** with tubulin, molecular docking studies were performed using LeDock software. The co-crystal structure of tubulin complexed with **ABT-751** [29] (PDB ID: 3HKC) was downloaded from RCSB protein bank (http://www.rcsb.org) and selected as the docking protein. Before the docking study started, we measured the feasibility of the docking model by redocking the native ligand **ABT-751** to the crystal structure (Fig. 7B), and the RMSD value of the best-docked pose was 0.540 Å, thus the docking method using LeDock was suitable. As shown in Fig. 7C, when focusing on the binding mode of the best docked pose of **HoAn32**, there are two hydrogen bonds formed between C≡N

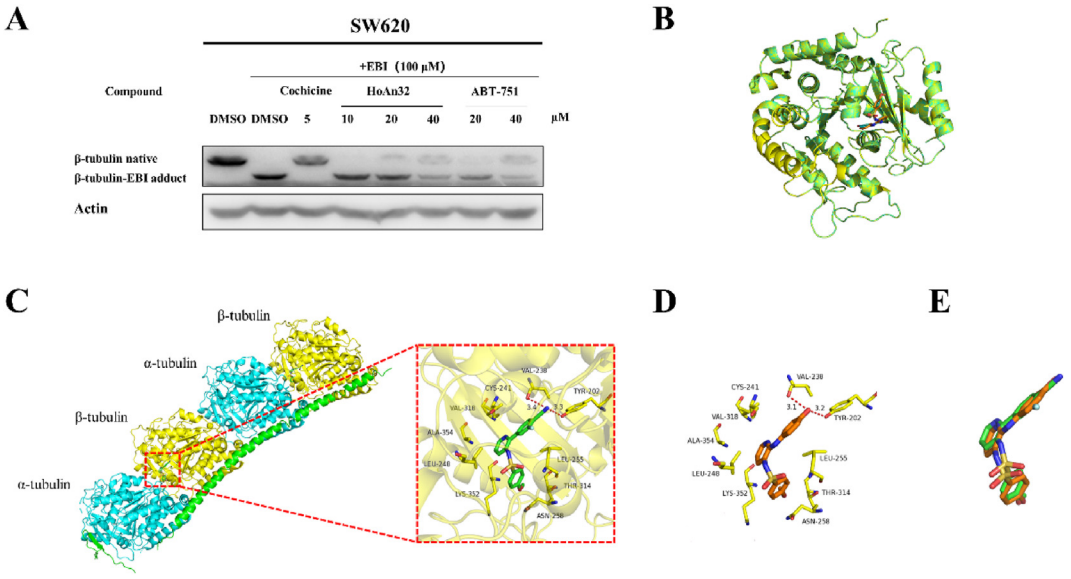

Fig. 7. Compound **HoAn32** binds in colchicine site of tubulin. (A). EBI competition assay. SW620 cells were incubated with **HoAn32** (0, 10 μM, 20 μM and 40 μM) and **ABT-751** (20 μM and 40 μM) for 2 h, followed by EBI (100 μM) for another 2 h. Then the β-tubulin and β-tubulin-EBI adducts were determined by western blot; (B). The redocking result of **ABT-751** with β-tubulin (PDB: 3HKC) (the orange stick represents the ligand in co-crystal structure and the blue stick represents the redocked ligand); (C). Proposed binding mode of **HoAn32** (shown in green stick) with tubulin (PDB: 3HKC); (D). The binding mode of **ABT-751** with tubulin (shown in orange stick); (E). Superimposition of **HoAn32** (green stick) and **ABT-751** (orange stick). (For interpretation of the references to colour in this figure legend, the reader is referred to the Web version of this article.)

group and Val-238 as well as Tyr-202 residues (3.4 Å and 3.3 Å, respectively) in the colchicine site from the tubulin β chain, and the binding mode of which was similar to the co-crystal structure of tubulin complexed with **ABT-751**, in which OH group also formed two hydrogen bonds (3.1 Å with Val-238 and 3.2 Å with Tyr-202) in the same place (Fig. 7D). Furthermore, when we superimposed **HoAn32** and **ABT-751**, the binding posture of them has a high similarity (Fig. 7E). These molecular docking results indicated that compound **HoAn32** tightly bind in the colchicine site and exhibit a strong polymerization inhibiting activity against tubulin, while the binding mode of **HoAn32** is different from colchicine with tubulin [29].

2.2.4. Compound HoAn32 induced G2/M cell cycle in human cancer cell lines

As most MTAs could disrupt the cell cycle distributions of cancer cells [30], we next detected the effect of **HoAn32** on the cell cycle of three different cancer cell lines by flow cytometer analysis. As shown in Fig. 8A and B, RKO, SW620 and PANC-1 cells were all arrested in the G2/M phase after treatment with **HoAn32** from 0 to 1 μM for 24 h, and the percentages of RKO, SW620 and PANC-1 cells in the G2/M phase were increased from 10.79% to 47.76%, 13.83% to 76.28% and 3.65% to 28.01%, respectively. The positive control **ABT-751** (1 μM) also showed the ability to disrupt cell cycle distributions, and the percentage of RKO and PANC-1 cells in the G2/M phase was reached 52.80% and 64.83%, respectively, while the effect on SW620 cells was not obvious after incubated with **ABT-751** at 1 μM for 24 h, the percentages of G2/M phase of which was 17.69%.

Activation of cdc2 kinase was an important event in mitosis of eukaryotic cells, which was controlled by several factors such as cyclin B1 and cdc25c, etc. [31] Thus, western blot assay was performed to detect the expression levels of cdc2 and cyclin B1 proteins in RKO and SW620 cells with the presence or absence of **HoAn32** to determine whether the effects on cell cycle was regulated by these factors. As depicted in Fig. 8C, the expression levels of cdc2 and cyclinB1 were gradually decreased after treatment with **HoAn32** from 0 to 1 μM for 24 h in both RKO and SW620 cells, while for ABT-751 treatment group, the expression level of cyclin B1 was also decreased in SW620 cells, and the effect was not obvious after incubated with **ABT-751** at 1 μM for 24 h.

2.2.5. Compound HoAn32 induced apoptosis in human cancer cell lines

The mitotic arrest of tumor cells by MTAs is generally associated with cellular apoptosis [32]. To evaluate the capacity of compound **HoAn32** to induce apoptosis in human cancer cell lines, FITC conjugated Annexin V/PI assay was performed in RKO and SW620 cells. As shown in Fig. 9A and B, after exposed to **HoAn32** from 0 to 1 μM for 24 h, the percentage of total apoptotic cells were increased from 3.39% to 38.17% in RKO cells, and from 6.07% to 14.35% in SW620 cells, while the percentage of which were 11.47% and 12.67% after incubated with **ABT-751** at 1 μM for 24 h, respectively.

Accumulating evidence has indicated that there exist some pivotal proteins such as Bcl-2 family (e.g. Bax, Bad and Bcl-2) and Caspase family (e.g. caspase-3, caspase-9) of proteins influence the process of cell apoptosis [33,34]. As illustrated in Fig. 9C, the level of Bax and cleaved PARP was efficiently up-regulated after treatment with **HoAn32** from 0 to 1 μM for 24 h, and the effect was also observed in **ABT-751** (1 μM) administration group. The above results revealed that compound **HoAn32** exert notable antiproliferative activity *in vitro*, display tubulin polymerization inhibition, and induce significant cell cycle arrest and cell apoptosis.

2.2.6. Compound HoAn32 induced ROS generation in human cancer cell lines

Growing evidence has indicated that increased levels of reactive oxygen species (ROS) in cancer cells play an important role in apoptosis induction [35,36]. Thus, the intracellular ROS levels were measured using the fluorescent probe 2′, 7′-dichlorofluorescein diacetate (DCFH-DA) in the presence or absence of compound **HoAn32** or **ABT-751** by flow cytometry. As shown in Fig. 10, after incubation with **HoAn32** at 0.25 μM and 0.5 μM for 24 h in SW620 cells, the ROS level elevated about 1.5 times compared with

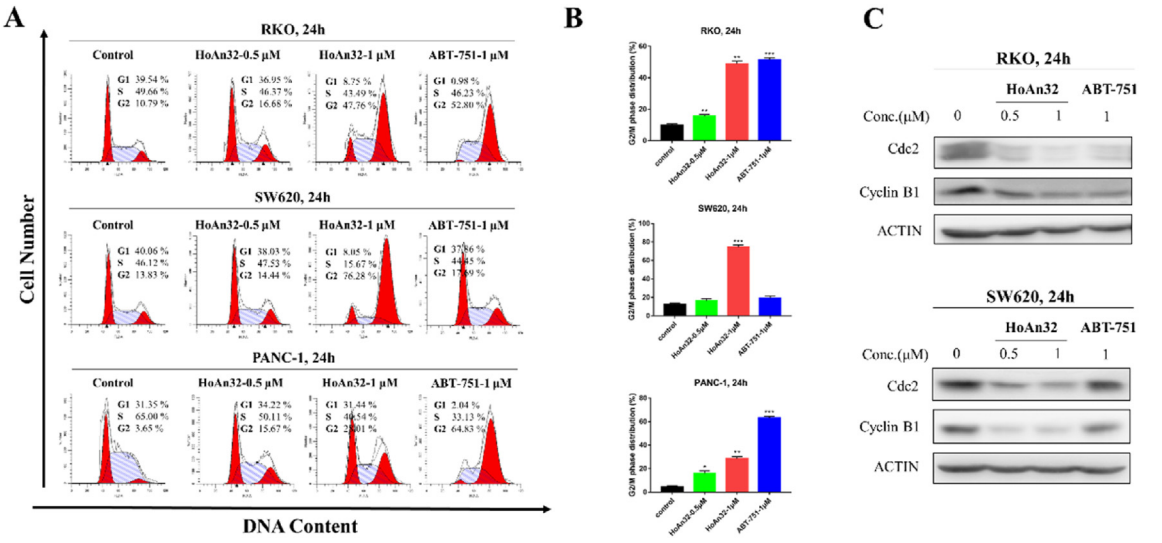

Fig. 8. Compound **HoAn32** induced G2/M phase arrest in different cancer cells. (A) RKO, SW620 and PANC-1 cells were treated with DMSO, **HoAn32** (0.5 μM and 1 μM) and **ABT-751** (1 μM) for 24 h. Cells were harvested and stained with PI, and then analyzed by flow cytometry. (B) The percentage of G2/M phase cell cycle distribution was displayed by histograms. (C) Western blot analysis was used to detect the expression of G2/M regulatory proteins. The experiments were performed at least three times, and the representative experiment results are shown. *$P < 0.05$, **$P < 0.01$, ***$P < 0.001$ vs control group.

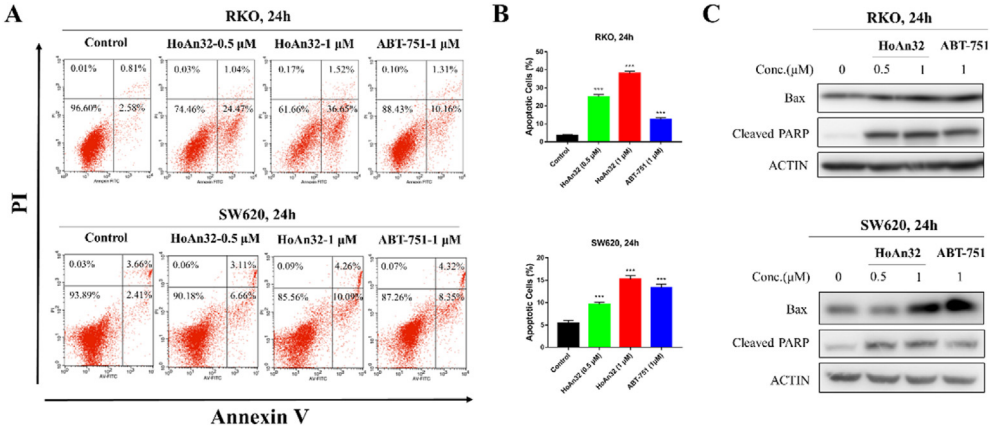

Fig. 9. Compound **HoAn32** induced apoptosis in different cancer cells. (A) RKO and SW620 cells were treated with DMSO, **HoAn32** (0.5 μM and 1 μM) and **ABT-751** (1 μM) for 24 h. The cells were collected and stained with PI/Annexin V, and then analyzed by flow cytometry. (B) The percentage of apoptotic cells was displayed by histograms. (C) Western blot analysis was used to detect the expression of apoptosis-related proteins. The experiments were performed at least three times, and the representative experiment results are shown. ***$P < 0.001$ vs control group.

the control group, while which was about 1.8 times for **ABT-751** (0.5 μM) treatment group. Similar results also appeared in RKO cells (Fig. 10). When cells exposure to 0.25 μM and 0.5 μM of **HoAn32**, the ROS level was elevated about 1.5 times compared with control group cells after treatment with **HoAn32** at 0.25 μM and 0.5 μM for 24 h and the relative ratio was about 2.0 times for **ABT-751** (0.5 μM) treatment group when compared with the control group. These results indicated that ROS mediated apoptosis in SW620 and RKO cells incubated with **HoAn32**.

2.2.7. Compound HoAn32 exhibited potent vascular disrupting activity

Most antitubulin agents possess anti-vascular activity, which contributed to the disruption of microtubule dynamics to induce endothelial cell shape change [37]. Considering the generation of new blood vessels are closely related to HUVEC migration [38], so the wound healing assay was performed to evaluate whether compound **HoAn32** possessed potent vascular disrupting activity. As shown in Fig. 11A, after treatment with **HoAn32** for 24 h, HUVEC migration was disturbed in a dose-dependent way from 0.5 μM to 1 μM when comparing with DMSO treatment group, and the wound closure percentage of which decreased from 71.8% to 20.1%, while the value of which was 18.0% for **ABT-751** (1 μM) treatment group (Fig. 11B).

In order to exclude the possibility that the anti-vascular activity of **HoAn32** was due to a cytotoxic action of **HoAn32**, we also determined the antiproliferative activity of **HoAn32** against HUVECs after a 24 h treatment by an MTS assay. The IC_{50} values of **HoAn32** and **ABT-751** against HUVECs were 8.9 ± 0.8 μM and 9.2 ± 1.1 μM, respectively, which are both higher than the concentration (1 μM) required for the obvious inhibition of cell migration. These results indicated that compound **HoAn32** possessed potent anti-vascular activity.

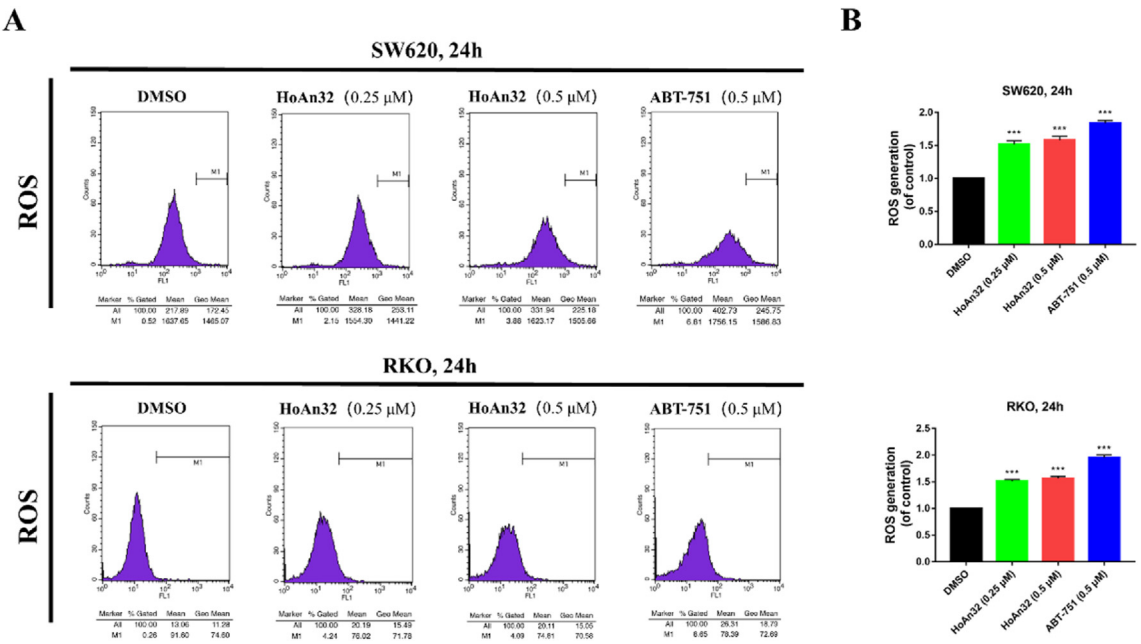

Fig. 10. Compound **HoAn32** induced ROS generation in SW620 and RKO cells. (A). ROS detecting fluorescent dye DCFH-DA was used to detect the generation of ROS in RKO and SW620 cells after incubation with **HoAn32** (0.25 μM and 0.5 μM) and **ABT-751** (0.5 μM) for 24 h, and then the ROS level was determined by flow cytometry. (B). The relative ratio of treatment group vs. control group was displayed by histograms. The experiments were performed at least three times, and the representative experiment results are shown. ***$P < 0.001$ vs control group.

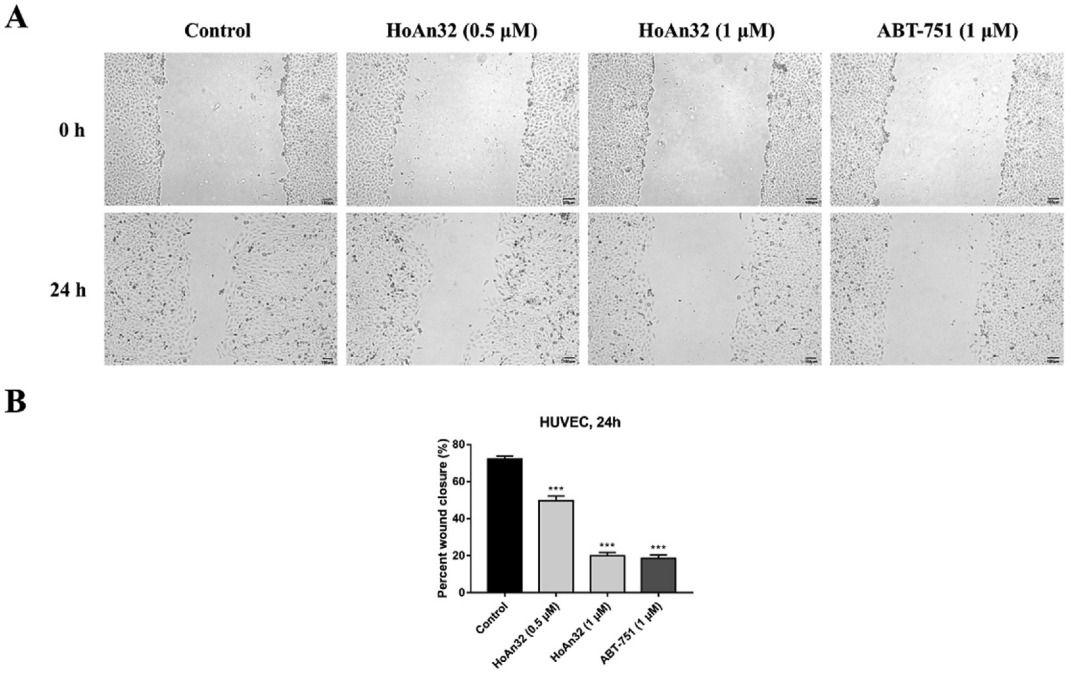

Fig. 11. Effects on HUVECs migration of compound **HoAn32**. (A). Sterile 200 μL pipette tips were used to produce scratches, and images were captured using inverted microscope at 0 and 24 h after treatments with 0, 0.5 μM, and 1 μM of **HoAn32** or 1 μM of **ABT-751**. (B). Histograms display the percent wound closure of the scratches at 0 and 24 h after treatments with 0, 0.5 μM, and 1 μM of **HoAn32** or 1 μM of **ABT-751**, ***$P < 0.001$ vs control group.

2.2.8. Physicochemical properties of Compound HoAn32

In order to evaluate the drug-likeness of compound **HoAn32**, we predicted the physicochemical properties of compound **HoAn32** using *DataWarrior* [39]. As shown in Table 3, compound **HoAn32** basically conformed to Lipinski's rules of five and owned moderate water solubility, and the parameters of which are similar with **ABT-751**.

2.2.9. Compound HoAn32 inhibited the growth of SW620 xenograft tumor in mice

Based on the excellent *in vitro* antiproliferative activity, compound **HoAn32** was selected to be evaluated *in vivo* antitumor activity using a SW620 xenograft model in nude mice, which was established by subcutaneous injection of SW620 cells into the right

Table 3
Physicochemical properties of compounds **HoAn32** and **ABT-751**.

Comp.	MW[a]	HBA[b]	HBD[c]	cLog *P*[d]	tPSA[e]	cLog S[f]
HoAn32	383.40	6	1	2.57	100.46	−5.03
ABT-751	371.41	7	3	2.42	108.93	−3.97
RO5[g]	<500	<10	<5	<5	<90	

[a] MW = molecular weight.
[b] HBA = hydrogen-bond acceptor atoms.
[c] HBD = hydrogen-bond donor atoms.
[d] cLog *P* = calculated logarithm of the octanol–water partition coefficient.
[e] tPSA = topological polar surface area.
[f] cLog S = calculated logarithm of the water solubility in mol/L, PH = 7.5, 25 °C, calculated using *DataWarrior* (http://www.openmolecules.org/datawarrior/).
[g] RO5 = Lipinski's rule of five.

armpit of mice. Once tumors reached about 100 mm^3 in volume, the mice were randomly allocated into three groups: vehicle (p.o., group 1), **HoAn32** (p.o., 25 mg/kg per 2 days, group 2), **ABT-751** (p.o., 25 mg/kg per 2 days, group 3), with six mice per group (Fig. 12A). As shown in Fig. 12B,D, after 20 days, the group receiving 25 mg/kg treatments of **HoAn32** reduced tumor growth by 53.6%, while the group receiving the same dose treatments of **ABT-751** achieved a tumor growth inhibition of 49.3%. The one-way ANOVA analysis followed by Dunnett's multiple comparison test also showed that there was a significant decrease compared to the control for both concentrations of **HoAn32**-treated groups ($P < 0.001$) and **ABT-751**-treated group ($P < 0.001$). Meanwhile, no significant body weight loss of mice was observed in **HoAn32** or **ABT-751** treatment group (Fig. 12C).

Additionally, H&E staining of the major organs including heart, liver, spleen, lung and kidney collected at the end of the study also indicated that there were no observable major organ-related toxicities after **HoAn32** treatment (Fig. 13). Overall, these data suggested that compound **HoAn32** was efficacious in inhibiting colon tumor growth *in vivo* with no observable toxicity.

3. Conclusions

In summary, we reported the design, synthesis and detailed SARs of a series of novel 2-aryl-3-sulfonamido-pyridines (**HoAns**). Among all these new compounds, **HoAn20** and **HoAn32** exhibited excellent broad-spectrum antiproliferative activities against a panel of human cancer cell lines *in vitro*. The IC_{50} values of compounds **HoAn20** and **HoAn32** were ranging from 0.204 μM to 2.457 μM, and from 0.170 μM to 1.193 μM, respectively. Further investigations of the optimal compound **HoAn32** found that it could induce tubulin depolymerization *in vitro* and bind in the colchicine site of β-tubulin, and molecular docking studies showed that compound **HoAn32** took a similar binding mode with tubulin comparing to the reference compound **ABT-751** [29]. Moreover, compound **HoAn32** induced colony formation inhibition, G2/M phase cell cycle arrest, cell apoptosis, and elevated the generation of ROS in both RKO and SW620 cells. In addition, compound **HoAn32** possessed potent vascular disrupting activity, which effectively inhibited HUVEC migration *in vitro*. Furthermore, the results from *in vivo* experiments indicated that compound **HoAn32** effectively inhibited tumor growth in mice SW620 xenograft models without observable toxicity. Collectively, our findings provide a new structure type as potential microtubule polymerization agents in cancer therapy field and the most active compound **HoAn32** deserves for further development in future.

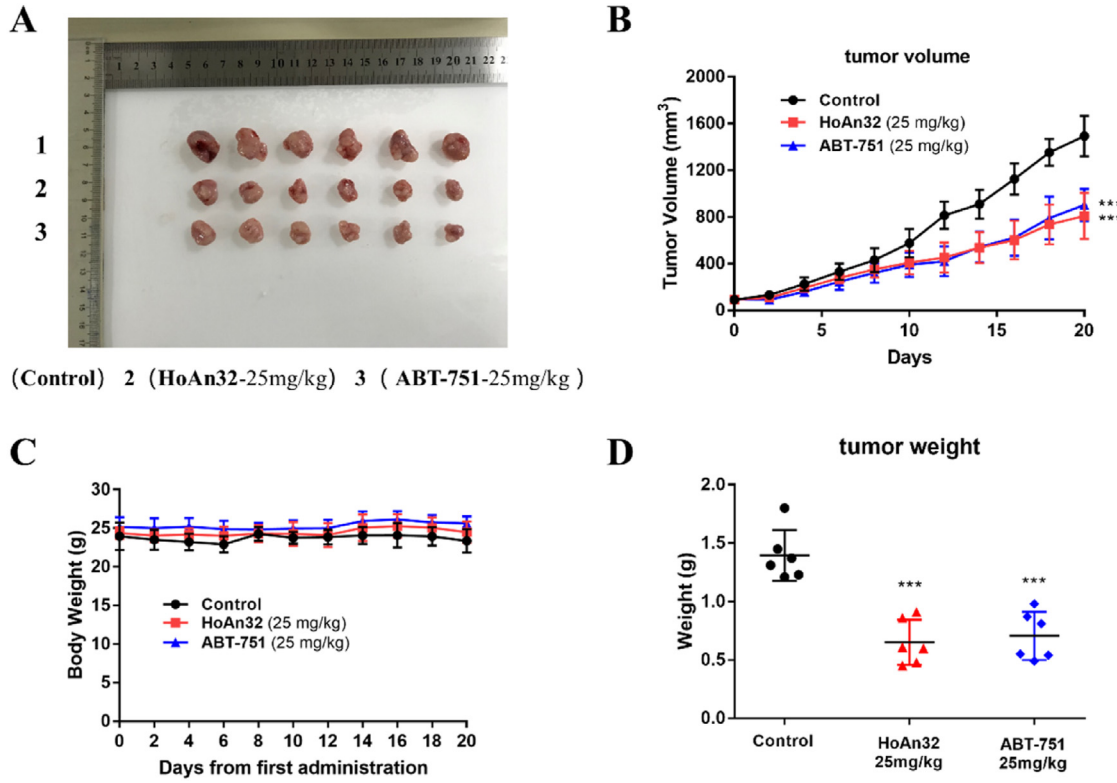

Fig. 12. Compound **HoAn32** showed antitumor activities in SW620 xenograft model. Nude mice bearing tumors formed by SW620 cells were administered with **HoAn32** (p.o., 25 mg/kg, per 2 days), **ABT-751** (p.o., 25 mg/kg, per 2 days), or vehicle. (A). Images of isolated tumors from mice at the end of observation. (B). Tumor volumes changes of nude mice (n = 6). (C). Body weight changes of mice during treatment. (D). Tumor weight of the individual tumors of each group. ***$P < 0.001$ vs control group.

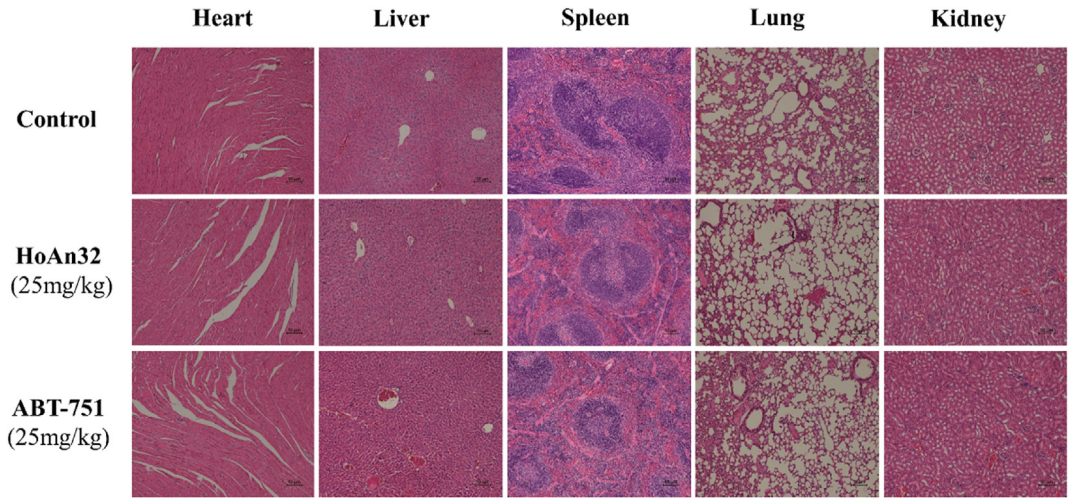

Fig. 13. H&E staining of major organs including heart, liver, spleen, lung and kidney of mice. No abnormality or apparent toxicities of these organs were observed.

4. Experimental section

4.1. Chemistry

General Methods. All solvents and reagents were commercially available and used without further purification. All reagents were weighed and handled in the air at room temperature. The reactions were monitored by thin-layer chromatography (TLC), which employed glass 0.25 mm silica gel plates (GF254) and visualized under UV light. Column chromatography was performed using 200−300 mesh silica gel (Qingdao Haiyang Chemical Co., Ltd, China). NMR Spectra were performed at 298 K, and all NMR spectra were recorded on Bruker AVANCE III 400 (Bruker Company, Germany) for ^{1}H NMR and ^{13}C NMR in the indicated solvents ($CDCl_3$ or DMSO-d_6). The NMR chemical shift was measured in δ (ppm) with residual solvent peaks as internal standards relative ($CDCl_3$, δ 7.26 ppm in ^{1}H NMR, δ 77.20 ppm in ^{13}C NMR; DMSO-d_6, δ 2.50 ppm in ^{1}H NMR, δ 39.52 ppm in ^{13}C NMR). Coupling constants (J) were reported in hertz, and the splitting abbreviations used were as follows: s, singlet; d, doublet; dd, doublet of doublets; t, triplet; m, multiplet; td, triplet of doublets; br.s, broad singlet. High-resolution mass spectra (HRMS) were tested on SHIMADZU LCMS-IT-TOF, which was equipped with an electrospray ion source (ESI) operating in positive or negative ion mode. Melting points were recorded with SGW®X-4A micro melting point apparatus (Shanghai INESA Physico-Optical Instrument Co., Ltd, China). High Performance Liquid Chromatography (HPLC) analysis was performed on an Agilent 1260 Infinity II LC system fitting with an Ultimate™ XB-C18 column (4.6 mm × 150 mm, 5 μm particle size) by using Acetonitrile-Water (v/v) mixture as eluent. The purities of all synthetic compounds were determined by HPLC analysis and was ≥95%.

Procedure A for Synthesizing of 4-methoxy-N-(2-(2-methoxyphenyl)pyridin-3-yl)benzenesulfonamide (HoAn1). 2-bromopyridin-3-amine (**1**) (500 mg, 2.89 mmol) and (2-methoxyphenyl)boronic acid (483 mg, 3.18 mmol) was dissolved in toluene/H_2O (2/1, v/v, 15 mL). Then, K_2CO_3 (1.6 g, 11.56 mmol) and $Pd(PPh_3)_4$ (167 mg, 0.145 mmol) were added, the reaction mixture was stirred at 80 °C for 8 h with N_2 atmosphere. The solvent was removed under reduced pressure, then the mixture was extracted with EA/H_2O (3/1, v/v, 50 mL) for three times and the EA layer was merged. The organic layer was dried with Na_2SO_4 and concentrated under reduced pressure to obtain the crude product. The crude product was purified by silica gel column chromatography (PE: EA = 2: 1) to give a yellowish solid 2-(2-methoxyphenyl) pyridin-3-amine (**2a**) (310 mg, 60%).

Compound **2a** (100 mg, 0.499 mmol) and DMAP (61 mg, 0.499 mmol) was dissolved in CH_2Cl_2 (8 mL), and pyridine (1 mL) was added subsequently. 4-methoxybenzenesulfonyl chloride (103 mg, 0.499 mmol) was added dropwise into the mixture at room temperature. Then, the mixture turned to 60 °C and stirred under reflux for 6 h. CH_2Cl_2 was removed and the mixture was extracted with EA/H_2O (3/1, v/v, 30 mL) for three times. The organic layer was collected and dried with Na_2SO_4, then concentrated under reduced pressure to obtain the crude product. The crude product was purified by silica gel column chromatography (PE: EA = 3: 1) to give a white solid **HoAn1** (122 mg, 66%). M.p: 130.1−130.8 °C. ^{1}H NMR (400 MHz, $CDCl_3$) (ppm): 8.51 (1H, dd, J_1 = 4.8 Hz, J_2 = 1.6 Hz, H-6), 8.00 (1H, dd, J_1 = 8.0 Hz, J_2 = 1.6 Hz, H-6′), 7.36-7.26 (2H, m, H-4, H-5), 7.16-7.12 (2H, m, H-2″, H-6″), 6.96 (1H, d, J = 8.0 Hz, H-3), 6.86 (1H, td, J_1 = 7.6 Hz, J_2 = 1.2 Hz, H-5′), 6.74 (1H, dd, J_1 = 7.6 Hz, J_2 = 1.6 Hz, H-4′), 6.62-6.58 (2H, m, H-3″, H-5″), 3.85 (3H, s, 2-OC$\underline{H}_3$), 3.80 (3H, s, 4″-OC$\underline{H}_3$). ^{13}C NMR (100 MHz, $CDCl_3$) (ppm): 162.8, 154.9, 151.5, 147.3, 133.8, 131.9, 131.6, 130.4, 130.1, 128.5 × 2, 126.6, 122.9, 121.7, 113.9 × 2, 111.3, 56.4, 55.5. HRMS (ESI, m/z) calcd. for $C_{19}H_{18}N_2O_4S$ $(M+H)^+$ 371.1060, found 371.1056. Purity: 99% by HPLC (t_R = 3.500 min).

Compounds **HoAn2**-**HoAn10**, **HoAn14**-**HoAn16**, **HoAn18** and **HoAn20**-**HoAn24** were prepared with a similar procedure which described for the synthesis of **HoAn1**.

4-methoxy-N-(2-(3-methoxyphenyl)pyridin-3-yl)benzenesulfonamide (HoAn2). White powder. Yield: 65%. M.p: 132.3−133.1 °C. ^{1}H NMR (400 MHz, DMSO-d_6) (ppm): 9.73 (1H, s,-N$\underline{H}$SO$_2$-), 8.48 (1H, dd, J_1 = 4.4 Hz, J_2 = 1.6 Hz, H-6), 7.54 (1H, dd, J_1 = 7.2 Hz, J_2 = 2.0 Hz, H-6′), 7.47 (2H, d, J = 8.8 Hz, H-2″, H-6″), 7.34-7.24 (2H, m, H-2, H-5), 7.07-7.00 (3H, m, H-4, H-4′, H-5′), 6.96 (2H, d, J = 8.8 Hz, H-3″, H-5″), 3.81 (3H, s, 3-OC$\underline{H}_3$), 3.76 (3H, s, 4″-OC$\underline{H}_3$). ^{13}C NMR (100 MHz, DMSO-d_6) (ppm): 163.8, 162.2, 147.1, 139.3, 134.9, 131.8, 131.0, 130.3, 128.7, 128.5 × 2, 122.8, 121.3, 114.4, 114.2 × 2, 113.8, 55.5, 54.9. HRMS (ESI, m/z) calcd. for $C_{19}H_{18}N_2O_4S$ $(M+H)^+$ 371.1060, found 371.1056. Purity: 99% by HPLC (t_R = 5.724 min).

4-methoxy-N-(2-(4-methoxyphenyl)pyridin-3-yl)benzenesulfonamide (HoAn3). Yellowish powder. Yield: 60%. M.p: 166.8−167.7 °C. ^{1}H NMR (400 MHz, $CDCl_3$) (ppm): 8.38 (1H, dd, J_1 = 4.8 Hz, J_2 = 1.6 Hz, H-6′), 8.01 (1H, dd, J_1 = 8.0 Hz, J_2 = 1.6 Hz, H-

4′), 7.53 (2H, d, J = 8.8 Hz, H-2, H-6), 7.23 (1H, dd, J_1 = 8.4 Hz, J_2 = 4.8 Hz, H-5′), 7.04 (2H, d, J = 8.8 Hz, H-2″, H-6″), 6.91 (2H, d, J = 8.8 Hz, H-3″, H-5″), 6.86 (2H, d, J = 8.8 Hz, H-3, H-5), 3.85 (3H, s, 4-OCH$_3$), 3.84 (3H, s, 4″-OCH$_3$). ^{13}C NMR (100 MHz, $CDCl_3$) (ppm): 163.4, 160.2, 150.9, 145.6, 131.5, 131.0, 130.2, 129.7 × 2, 129.2 × 2, 128.9, 122.7, 114.6 × 2, 114.3 × 2, 55.6, 55.4. HRMS (ESI, *m/z*) calcd. for $C_{19}H_{18}N_2O_4S$ $(M+H)^+$ 371.1060, found 371.1058. Purity: 95% by HPLC (t_R = 5.516 min).

N-(2-(2,3-dimethoxyphenyl)pyridin-3-yl)-4-methoxybenzenesulfonamide (HoAn4). White powder. Yield: 63%. M.p: 106.8–107.7 °C. ^{1}H NMR (400 MHz, DMSO-d_6) (ppm): 8.92 (1H, s, -NHSO$_2$-), 8.42 (1H, dd, J_1 = 8.8 Hz, J_2 = 1.2 Hz, H-6), 7.63 (1H, dd, J_1 = 8.4 Hz, J_2 = 1.2 Hz, H-6′), 7.42 (2H, d, J = 8.8 Hz, H-2″, H-6″), 7.36 (1H, dd, J_1 = 8.0 Hz, J_2 = 4.8 Hz, H-5), 7.08 (1H, dd, J_1 = 8.4 Hz, J_2 = 1.2 Hz, H-4), 6.98 (1H, t, J = 8.0 Hz, H-5′), 6.93 (2H, d, J = 8.8 Hz, H-3″, H-5″), 6.41 (1H, dd, J_1 = 7.8 Hz, J_2 = 1.2 Hz, H-4′), 3.85 (3H, s, 2-OCH$_3$), 3.80 (3H, s, 3-OCH$_3$), 3.50 (3H, s, 4″-OCH$_3$). ^{13}C NMR (100 MHz, DMSO-d_6) (ppm): 162.4, 152.2, 151.5, 146.1, 145.7, 132.0, 131.9, 131.4, 131.1, 128.4 × 2, 123.6, 122.9, 122.5, 114.2 × 2, 113.0, 60.6, 55.7, 55.6. HRMS (ESI, *m/z*) calcd. for $C_{20}H_{20}N_2O_5S$ $(M+H)^+$ 401.1166, found 401.1174. Purity: 96% by HPLC (t_R = 3.717 min).

N-(2-(2,4-dimethoxyphenyl)pyridin-3-yl)-4-methoxybenzenesulfinamide (HoAn5). Yellowish oil. Yield: 59%. ^{1}H NMR (400 MHz, DMSO-d_6) (ppm): 8.66 (1H, s, -NHSO$_2$-), 8.38 (1H, dd, J_1 = 8.8 Hz, J_2 = 1.2 Hz, H-6), 7.60 (1H, dd, J_1 = 8.4 Hz, J_2 = 1.2 Hz, H-6′), 7.40 (2H, d, J = 9.2 Hz, H-2″, H-6″), 7.30 (1H, dd, J_1 = 8.0 Hz, J_2 = 4.8 Hz, H-5), 6.92 (2H, d, J = 8.8 Hz, H-3″, H-5″), 6.72 (1H, d, J = 8.0 Hz, H-5′), 6.58 (1H, d, J = 2.4 Hz, H-3), 6.45 (1H, dd, J_1 = 8.4 Hz, J_2 = 2.4 Hz, H-4′), 3.82 (3H, s, 4-OCH$_3$), 3.81 (3H, s, 4″-OCH$_3$), 3.72 (3H, s, 2-OCH$_3$). ^{13}C NMR (100 MHz, DMSO-d_6) (ppm): 162.3, 160.8, 156.9, 151.7, 146.2, 131.9, 131.8, 131.7, 131.4, 128.4 × 2, 122.4, 119.3, 114.1 × 2, 105.1, 98.1, 55.6 × 2, 55.2. HRMS (ESI, *m/z*) calcd. for $C_{20}H_{20}N_2O_5S$ $(M+H)^+$ 401.1166, found 401.1168. Purity: 99% by HPLC (t_R = 3.526 min).

N-(2-(2,5-dimethoxyphenyl)pyridin-3-yl)-4-methoxybenzenesulfonamide (HoAn6). White powder. Yield: 54%. M.p: 110.1–110.9 °C. ^{1}H NMR (400 MHz, DMSO-d_6) (ppm): 8.54 (1H, s, -NHSO$_2$-), 8.44 (1H, dd, J_1 = 8.8 Hz, J_2 = 1.2 Hz, H-6′), 7.66 (1H, dd, J_1 = 8.0 Hz, J_2 = 1.6 Hz, H-6), 7.38 (1H, dd, J_1 = 8.0 Hz, J_2 = 4.8 Hz, H-3), 7.29 (2H, d, J = 8.8 Hz, H-2″, H-6″), 7.01-6.92 (2H, m, H-4, H-5′), 6.86 (2H, d, J = 8.8 Hz, H-3″, H-5″), 6.28 (1H, d, J = 3.2 Hz, H-4′), 3.79 (3H, s, 5-OCH$_3$), 3.69 (3H, s, 4″-OCH$_3$), 3.64 (3H, s, 2-OCH$_3$). ^{13}C NMR (100 MHz, DMSO-d_6) (ppm): 162.3, 152.9, 151.8, 149.5, 146.7, 133.2, 131.5, 131.0, 128.3 × 2, 127.2, 122.9, 116.0, 115.0, 114.1 × 2, 112.5, 56.2, 55.4, 55.1. HRMS (ESI, *m/z*) calcd. for $C_{20}H_{20}N_2O_5S$ $(M+H)^+$ 401.1166, found 401.1172. Purity: 98% by HPLC (t_R = 3.603 min).

N-(2-(2,6-dimethoxyphenyl)pyridin-3-yl)-4-methoxybenzenesulfonamide (HoAn7). White powder. Yield: 48%. M.p: 145.0–145.8 °C. ^{1}H NMR (400 MHz, DMSO-d_6) (ppm): 8.77 (1H, s, -NHSO$_2$-), 8.27 (1H, dd, J_1 = 8.8 Hz, J_2 = 1.2 Hz, H-6′), 7.63 (2H, d, J = 8.8 Hz, H-2″, H-6″), 7.60 (1H, dd, J_1 = 8.4 Hz, J_2 = 1.2 Hz, H-4), 7.35 (1H, t, J = 8.4 Hz, H-5′), 7.22 (1H, dd, J_1 = 8.4 Hz, J_2 = 4.8 Hz, H-4′), 7.02 (2H, d, J = 8.8 Hz, H-3″, H-5″), 6.67 (2H, d, J = 8.4 Hz, H-3, H-5), 3.81 (3H, s, 4″-OCH$_3$), 3.55 (6H, s, 2-OCH$_3$, 6-OCH$_3$). ^{13}C NMR (100 MHz, DMSO-d_6) (ppm): 162.3, 157.8 × 2, 147.4, 144.8, 133.1, 132.0, 131.5, 130.0, 128.7 × 2, 128.2, 122.3, 114.2 × 2, 103.9 × 2, 55.6, 55.4 × 2. HRMS (ESI, *m/z*) calcd. for $C_{20}H_{20}N_2O_5S$ $(M+H)^+$ 401.1166, found 401.1164. Purity: 99% by HPLC (t_R = 2.906 min).

N-(2-(3,4-dimethoxyphenyl)pyridin-3-yl)-4-methoxybenzenesulfonamide (HoAn8). Yellowish powder. Yield: 52%. M.p: 161.8–162.6 °C. ^{1}H NMR (400 MHz, DMSO-d_6) (ppm): 9.72 (1H, s, -NHSO$_2$-), 8.46 (1H, dd, J_1 = 8.8 Hz, J_2 = 1.2 Hz, H-6′), 7.46 (2H, d, J = 8.8 Hz, H-2″, H-6″), 7.43 (1H, dd, J_1 = 8.4 Hz, J_2 = 1.2 Hz, H-6), 7.27 (1H, dd, J_1 = 8.0 Hz, J_2 = 4.4 Hz, H-5′), 7.14 (1H, dd, J_1 = 8.4 Hz, J_2 = 2.0 Hz, H-4′), 7.09 (1H, s, H-2), 6.95-6.91 (3H, m, H-5, H-3″, H-5″), 3.81 (3H, s, 3-OCH$_3$), 3.80 (3H, s, 4-OCH$_3$), 3.73 (3H, s, 4″-OCH$_3$). ^{13}C NMR (100 MHz, DMSO-d_6) (ppm): 162.1, 154.7, 148.8, 148.0, 147.1, 135.1, 132.0, 130.4, 130.0, 128.5 × 2, 122.2, 121.7, 114.1 × 2, 112.6, 110.8, 55.5, 55.4, 55.2. HRMS (ESI, *m/z*) calcd. for $C_{20}H_{20}N_2O_5S$ $(M+H)^+$ 401.1166, found 401.1163. Purity: 98% by HPLC (t_R = 7.658 min).

N-(2-(3,5-dimethoxyphenyl)pyridin-3-yl)-4-methoxybenzenesulfonamide (HoAn9). White powder. Yield: 61%. M.p: 148.3–149.2 °C. ^{1}H NMR (400 MHz, DMSO-d_6) (ppm): 9.73 (1H, s, -NHSO$_2$-), 8.47 (1H, dd, J_1 = 8.4 Hz, J_2 = 1.6 Hz, H-6′), 7.49 (1H, dd, J_1 = 8.0 Hz, J_2 = 1.6 Hz, H-4′), 7.46 (2H, d, J = 8.8 Hz, H-2″, H-6″), 7.33 (1H, dd, J_1 = 8.0 Hz, J_2 = 4.8 Hz, H-5′), 6.95 (2H, d, J = 8.8 Hz, H-3″, H-5″), 6.92 (2H, d, J = 2.0 Hz, H-2, H-6), 6.49 (1H, t, J = 2.0 Hz, H-4), 3.81 (3H, s, 4″-OCH$_3$), 3.74 (6H, s, 3-OCH$_3$, 5-OCH$_3$). ^{13}C NMR (100 MHz, DMSO-d_6) (ppm): 162.2, 159.8 × 2, 154.7, 147.0, 139.7, 135.1, 131.9, 130.2, 128.5 × 2, 122.9, 114.1 × 2, 107.1 × 2, 100.2, 55.5, 55.1 × 2. HRMS (ESI, *m/z*) calcd. for $C_{20}H_{20}N_2O_5S$ $(M+H)^+$ 401.1166, found 401.1171. Purity: 96% by HPLC (t_R = 3.391 min).

4-methoxy-N-(2-(3,4,5-trimethoxyphenyl)pyridin-3-yl)benzenesulfonamide (HoAn10). Yellowish powder. Yield: 58%. M.p: 143.6–144.5 °C. ^{1}H NMR (400 MHz, DMSO-d_6) (ppm): 9.79 (1H, s, -NHSO$_2$-), 8.48 (1H, dd, J_1 = 8.4 Hz, J_2 = 1.6 Hz, H-6′), 7.49 (1H, dd, J_1 = 8.4 Hz, J_2 = 1.6 Hz, H-4′), 7.46 (2H, d, J = 8.8 Hz, H-2″, H-6″), 7.33 (1H, dd, J_1 = 8.0 Hz, J_2 = 4.8 Hz, H-5′), 6.94 (2H, d, J = 8.8 Hz, H-3″, H-5″), 6.80 (2H, s, H-2, H-6), 3.80 (3H, s, 4″-OCH$_3$), 3.76 (6H, s, 3-OCH$_3$, 5-OCH$_3$), 3.72 (3H, s, 4-OCH$_3$). ^{13}C NMR (100 MHz, DMSO-d_6) (ppm): 162.1, 154.8, 152.2 × 2, 147.1, 137.5, 135.5, 133.2, 132.1, 130.0, 128.4 × 2, 122.7, 114.1 × 2, 106.6 × 2, 59.9, 55.7 × 2, 55.5. HRMS (ESI, *m/z*) calcd. for $C_{21}H_{22}N_2O_6S$ $(M+H)^+$ 431.1271, found 431.1268. Purity: 95% by HPLC (t_R = 4.579 min).

N-(2-(4-(benzyloxy)phenyl)pyridin-3-yl)-4-methoxybenzenesulfonamide (HoAn14). Yellowish powder. Yield: 68%. M.p: 109.9–110.8 °C. ^{1}H NMR (400 MHz, DMSO-d_6) (ppm): 9.71 (1H, s, -NHSO$_2$-), 8.44 (1H, dd, J_1 = 8.4 Hz, J_2 = 1.2 Hz, H-6′), 7.51-7.40 (10H, m, 5H-benzyloxy, H-2, H-6, H-4′, H-2″, H-6″), 7.25 (1H, dd, J_1 = 8.0 Hz, J_2 = 4.8 Hz, H-5′), 6.99 (2H, d, J = 8.8 Hz, H-3, H-5), 6.95 (2H, d, J = 8.8 Hz, H-3″, H-5″), 5.15 (2H, s, -OCH$_2$-phenyl), 3.80 (3H, s, 4″-OCH$_3$). ^{13}C NMR (100 MHz, DMSO-d_6) (ppm): 162.2, 158.2, 154.6, 147.0, 137.0, 134.8, 131.9, 130.4 × 2, 129.4, 128.6 × 2, 128.4 × 2, 127.8, 127.7 × 2, 127.6, 122.2, 114.2 × 2, 113.9 × 2, 69.1, 55.6. HRMS (ESI, *m/z*) calcd. for $C_{25}H_{22}N_2O_4S$ $(M+H)^+$ 447.1373, found 447.1380. Purity: 95% by HPLC (t_R = 17.378 min).

4-methoxy-N-(2-(4-(trifluoromethyl)phenyl)pyridin-3-yl) benzenesulfonamide (HoAn15). Yellowish powder. Yield: 56%. M.p: 165.5–166.3 °C. ^{1}H NMR (400 MHz, DMSO-d_6) (ppm): 9.90 (1H, s, -NHSO$_2$-), 8.53 (1H, dd, J_1 = 8.4 Hz, J_2 = 1.2 Hz, H-6′), 7.71 (2H, d, J = 8.8 Hz, H-2, H-6), 7.68 (2H, d, J = 8.4 Hz, H-3, H-5), 7.50 (1H, dd, J_1 = 8.0 Hz, J_2 = 1.6 Hz, H-4′), 7.45 (2H, d, J = 8.8 Hz, H-2″, H-6″), 7.39 (1H, dd, J_1 = 8.0 Hz, J_2 = 4.4 Hz, H-5′), 6.95 (2H, d, J = 8.8 Hz, H-3″, H-5″), 3.80 (3H, s, 4″-OCH$_3$). ^{13}C NMR (100 MHz, DMSO-d_6) (ppm): 162.3, 153.6, 147.5, 135.4, 134.6, 131.4, 130.6, 129.8 × 2, 128.6 × 4, 124.6, 124.5, 123.6, 114.2 × 2, 55.5. HRMS (ESI, *m/z*) calcd. for $C_{19}H_{15}F_3N_2O_3S$ $(M+H)^+$ 409.0828, found 409.0833. Purity: 98% by HPLC (t_R = 2.851 min).

4-methoxy-N-(2-(4-nitrophenyl)pyridin-3-yl)benzenesulfonamide (HoAn16). Yellowish powder. Yield: 50%. M.p: 170.2–171.1 °C. ^{1}H NMR (400 MHz, DMSO-d_6) (ppm): 9.94 (1H, s, -NHSO$_2$-), 8.56 (1H, dd, J_1 = 8.4 Hz, J_2 = 1.2 Hz, H-6′), 8.20 (2H, d, J = 8.8 Hz, H-2, H-6), 7.74 (2H, d, J = 8.4 Hz, H-3, H-5), 7.51 (1H, d, J = 7.2 Hz, H-4′), 7.43-7.41 (3H, m, H-5′, H-2″, H-6″), 6.94 (2H, d, J = 8.8 Hz, H-3″, H-5″), 3.80 (3H, s, 4″-OCH$_3$). ^{13}C NMR (100 MHz,

DMSO-d_6) (ppm): 162.4, 153.1, 147.7, 146.9, 144.7, 135.9, 131.2, 130.8, 130.3 × 2, 128.6 × 2, 124.0, 122.8 × 2, 114.2 × 2, 55.5. HRMS (ESI, *m/z*) calcd. for $C_{18}H_{15}N_3O_5S$ $(M+H)^+$ 386.0805, found 386.0801. Purity: 99% by HPLC (t_R = 6.279 min).

4-methoxy-N-(2-(3-nitrophenyl)pyridin-3-yl)benzenesulfonamide (HoAn18). Yellowish powder. Yield: 52%. M.p: 185.1–185.9 °C. ^{1}H NMR (400 MHz, DMSO-d_6) (ppm): 9.97 (1H, s, -NHSO$_2$-), 8.57 (1H, dd, J_1 = 4.8 Hz, J_2 = 1.6 Hz, H-6), 8.22-8.20 (2H, m, H-2, H-4), 7.97 (1H, d, J = 7.6 Hz, H-6′), 7.68-7.63 (1H, m, H-5), 7.56 (1H, dd, J_1 = 8.0 Hz, J_2 = 1.6 Hz, H-4′), 7.44 (1H, dd, J_1 = 8.0 Hz, J_2 = 4.8 Hz, H-5′), 7.36 (2H, d, J = 9.2 Hz, H-2″, H-6″), 6.89 (2H, d, J = 8.8 Hz, H-3″, H-5″), 3.77 (3H, s, 4″-OCH$_3$). ^{13}C NMR (100 MHz, DMSO-d_6) (ppm): 162.3, 153.1, 147.9, 147.3, 139.6, 136.6, 135.4, 131.1, 130.5, 129.3, 128.5 × 2, 123.9, 123.6, 122.8, 114.1 × 2, 55.5. HRMS (ESI, *m/z*) calcd. for $C_{18}H_{15}N_3O_5S$ $(M+H)^+$ 386.0805, found 386.0793. Purity: 96% by HPLC (t_R = 6.072 min).

N-(2-(4-cyanophenyl)pyridin-3-yl)-4-methoxybenzenesulfonamide (HoAn20). White powder. Yield: 50%. M.p: 208.0–208.8 °C. ^{1}H NMR (400 MHz, DMSO-d_6) (ppm): 9.90 (1H, s, -NHSO$_2$-), 8.54 (1H, dd, J_1 = 8.4 Hz, J_2 = 1.2 Hz, H-6′), 7.82 (2H, d, J = 8.4 Hz, H-2, H-6), 7.65 (2H, d, J = 8.4 Hz, H-3, H-5), 7.49 (1H, dd, J_1 = 8.4 Hz, J_2 = 1.6 Hz, H-4′), 7.43 (2H, d, J = 8.8 Hz, H-2″, H-6″), 7.39 (1H, dd, J_1 = 8.0 Hz, J_2 = 4.4 Hz, H-5′), 6.96 (2H, d, J = 9.2 Hz, H-3″, H-5″), 3.82 (3H, s, 4″-OCH$_3$). ^{13}C NMR (100 MHz, DMSO-d_6) (ppm): 162.4, 153.4, 147.6, 142.7, 135.7, 131.7 × 2, 131.3, 130.7, 129.9 × 2, 128.6 × 2, 123.8, 118.8, 114.2 × 2, 110.6, 55.6. HRMS (ESI, *m/z*) calcd. for $C_{19}H_{15}N_3O_3S$ $(M+H)^+$ 366.0907, found 366.0907. Purity: 98% by HPLC (t_R = 2.931 min).

N-(2-(3-cyanophenyl)pyridin-3-yl)-4-methoxybenzenesulfonamide (HoAn21). White powder. Yield: 62%. M.p: 200.2–201.1 °C. ^{1}H NMR (400 MHz, CDCl$_3$) (ppm): 8.47 (1H, d, J = 4.0 Hz, H-6), 8.09 (1H, d, J = 8.4 Hz, H-6′), 7.67 (1H, d, J = 6.8 Hz, H-4), 7.53-7.46 (4H, m, H-5, H-4′, H-2″, H-6″), 7.36 (1H, dd, J_1 = 8.0 Hz, J_2 = 4.4 Hz, H-5′), 7.08 (1H, s, H-2), 6.93 (2H, d, J = 8.4 Hz, H-3″, H-5″), 6.55 (1H, s, -NHSO$_2$-), 3.89 (3H, s, 4″-OCH$_3$). ^{13}C NMR (100 MHz, CDCl$_3$) (ppm): 163.7, 149.8, 146.6, 137.9, 132.9, 132.4, 132.1, 131.8, 131.0, 129.9, 129.8, 129.0 × 2, 124.0, 117.9, 114.7 × 2, 113.2, 55.8. HRMS (ESI, *m/z*) calcd. for $C_{19}H_{15}N_3O_3S$ $(M+H)^+$ 366.0907, found 366.0910. Purity: 95% by HPLC (t_R = 5.004 min).

N-(2-(benzo[d][1,3]dioxol-5-yl)pyridin-3-yl)-4-methoxybenzenesulfonamide (HoAn22). Yellowish powder. Yield: 67%. M.p: 170.9–171.8 °C. ^{1}H NMR (400 MHz, DMSO-d_6) (ppm): 9.69 (1H, s, -NHSO$_2$-), 8.44 (1H, d, J = 3.6 Hz, H-6′), 7.47 (1H, d, J = 6.4 Hz, H-6), 7.45 (2H, d, J = 8.4 Hz, H-2″, H-6″), 7.29 (1H, dd, J_1 = 8.0 Hz, J_2 = 4.8 Hz, H-5′), 6.99-6.93 (4H, m, H-2, H-5, H-3″, H-5″), 6.87 (1H, d, J = 8.0 Hz, H-4′), 6.05 (2H, s, -OCH$_2$O-), 3.81 (3H, s, 4″-OCH$_3$). ^{13}C NMR (100 MHz, DMSO-d_6) (ppm): 162.3, 154.6, 147.1, 146.7, 135.4, 131.9, 131.8, 131.0, 130.0, 128.5 × 2, 123.1, 122.5, 114.1 × 2, 109.3, 107.6, 101.0, 55.5. HRMS (ESI, *m/z*) calcd. for $C_{19}H_{16}N_2O_5S$ $(M+H)^+$ 385.0853, found 385.0862. Purity: 99% by HPLC (t_R = 5.291 min).

N-(2-(dibenzo[b,d]furan-4-yl)pyridin-3-yl)-4-methoxybenzenesulfonamide (HoAn23). White powder. Yield: 61%. M.p: 162.3–163.2 °C. ^{1}H NMR (400 MHz, DMSO-d_6) (ppm): 9.67 (1H, s, -NHSO$_2$-), 8.54 (1H, dd, J_1 = 4.4 Hz, J_2 = 1.2 Hz, H-6′), 8.16 (1H, d, J = 8.0 Hz, H-6), 8.14 (1H, d, J = 7.6 Hz, H-4), 7.72 (1H, dd, J_1 = 8.0 Hz, J_2 = 1.6 Hz, H-5(benzofuran)), 7.61 (1H, d, J = 8.0 Hz, H-2(benzofuran)), 7.53-7.35 (6H, m, H-5, H-5′, H-2″, H-6″, H-3(benzofuran), H-4(benzofuran)), 7.24 (1H, dd, J_1 = 7.2 Hz, J_2 = 1.2 Hz, H-4′), 6.77 (2H, d, J = 8.8 Hz, H-3″, H-5″), 3.60 (3H, s, 4″-OCH$_3$). ^{13}C NMR (100 MHz, DMSO-d_6) (ppm): 162.0, 155.4, 153.0, 150.8, 146.8, 134.1, 131.7, 131.4, 128.3 × 2, 128.2, 127.4, 123.9, 123.5, 123.5, 122.9, 122.6, 122.3, 121.1, 121.0, 113.9 × 2, 111.6, 55.3. HRMS (ESI, *m/z*) calcd. for $C_{24}H_{18}N_2O_4S$ $(M+H)^+$ 431.1060, found 431.1060. Purity: 98% by HPLC (t_R = 5.354 min).

4-methoxy-N-(2-phenylpyridin-3-yl)benzenesulfonamide (HoAn24). White powder. Yield: 83%. M.p: 141.6–142.5 °C. ^{1}H NMR (400 MHz, DMSO-d_6) (ppm): 9.74 (1H, s, -NHSO$_2$-), 8.48 (1H, dd, J_1 = 4.8 Hz, J_2 = 1.6 Hz, H-6′), 7.52-7.45 (5H, m, H-2, H-4, H-6, H-2″, H-6″), 7.38-7.35 (3H, m, H-3, H-5, H-4′), 7.31 (1H, dd, J_1 = 8.0 Hz, J_2 = 4.4 Hz, H-5′), 6.98 (2H, d, J = 8.8 Hz, H-3″, H-5″), 3.81 (3H, s, 4″-OCH$_3$). ^{13}C NMR (100 MHz, DMSO-d_6) (ppm): 162.3, 154.8, 147.0, 138.1, 134.5, 131.8, 130.4, 129.0 × 2, 128.6 × 2, 128.0, 127.7 × 2, 122.7, 114.3 × 2, 55.6. HRMS (ESI, *m/z*) calcd. for $C_{18}H_{16}N_2O_3S$ $(M+H)^+$ 341.0954, found 341.0939. Purity: 98% by HPLC (t_R = 3.141 min).

Procedure B for Synthesizing of N-(2-(2-hydroxyphenyl)pyridin-3-yl)-4-methoxybenzenesulfonamide (HoAn11). 2-bromopyridin-3-amine (**1**) (500 mg, 2.89 mmol), pyridine (1 mL) and DMAP (176 mg, 1.44 mmol) was dissolved in CH_2Cl_2, and then 4-methoxybenzenesulfonyl chloride (716 mg, 3.47 mmol) was added slowly, the reaction mixture was stirred under reflux at 66 °C for 10 h. After that, CH_2Cl_2 was removed under reduced pressure and extracted with EA/H_2O (2/1, v/v, 400 mL) for three times, the EA layer was converged and removed to give the crude product. The crude product was purified by silica gel column chromatography (PE: EA = 6: 1) to obtain a yellowish solid N-(2-bromopyridin-3-yl)-4-methoxybenzenesulfonamide (**2**) (793 mg, 80%).

Compound **2** (200 mg, 0.582 mmol) and (2-hydroxyphenyl) boronic acid (80 mg, 0.582 mmol) was dissolved in THF/H_2O (2/1, v/v, 15 mL), and then $Pd(PPh_3)_4$ (34 mg, 0.029 mmol) and K_2CO_3 (121 mg, 0.874 mmol) was added. The mixture was stirred under reflux at 70 °C for 5 h. When the reaction finished, the solvent was removed under reduced pressure and extracted with EA/H_2O (1/1, v/v, 300 mL) for three times. The organic layer was concentrated and purified by silica gel column chromatography (PE: EA = 2: 1). A yellowish solid **HoAn11** (102 mg, 49%) was obtained. M.p: 150.8–151.6 °C. ^{1}H NMR (400 MHz, DMSO-d_6) (ppm): 10.80 (1H, s, -NHSO$_2$-), 8.62 (1H, s, 2-OH), 8.48 (1H, d, J = 3.6 Hz, H-6), 7.73 (1H, dd, J_1 = 8.0 Hz, J_2 = 1.2 Hz, H-6′), 7.40 (1H, dd, J_1 = 8.0 Hz, J_2 = 4.4 Hz, H-5′), 7.23 (1H, t, J = 8.4 Hz, H-4), 7.15 (2H, d, J = 8.8 Hz, H-2″, H-6″), 6.94 (1H, d, J = 8.4 Hz, H-5), 6.83 (1H, d, J = 6.8 Hz, H-3), 6.75 (2H, d, J = 8.8 Hz, H-3″, H-5″), 6.72 (1H, d, J = 7.6 Hz, H-4′), 3.77 (3H, s, 4″-OCH$_3$). ^{13}C NMR (100 MHz, DMSO-d_6) (ppm): 162.4, 152.8, 147.0, 146.9, 133.8, 131.7, 129.9, 128.7, 128.6, 128.0 × 2, 124.7, 122.7, 119.4, 115.6, 114.1 × 2, 55.5. HRMS (ESI, *m/z*) calcd. for $C_{18}H_{16}N_2O_4S$ $(M+H)^+$ 357.0904, found 357.0896. Purity: 98% by HPLC (t_R = 4.174 min).

Compounds **HoAn12** and **HoAn13** were prepared with a similar procedure which described for the synthesis of **HoAn11**.

N-(2-(3-hydroxyphenyl)pyridin-3-yl)-4-methoxybenzenesulfonamide (HoAn12). White powder. Yield: 55%. M.p: 185.8–186.6 °C. ^{1}H NMR (400 MHz, DMSO-d_6) (ppm): 9.64 (1H, s, -NHSO$_2$-), 9.42 (1H, s, 3-OH), 8.43 (1H, dd, J_1 = 8.4 Hz, J_2 = 1.2 Hz, H-6′), 7.54 (2H, d, J = 8.8 Hz, H-2″, H-6″), 7.43 (1H, dd, J_1 = 8.0 Hz, J_2 = 1.2 Hz, H-6), 7.27 (1H, dd, J_1 = 8.0 Hz, J_2 = 4.8 Hz, H-5′), 7.15 (1H, t, J = 8.4 Hz, H-5), 6.99 (2H, d, J = 8.8 Hz, H-3″, H-5″), 6.91-6.90 (2H, m, H-2, H-4), 6.77 (1H, dd, J_1 = 8.4 Hz, J_2 = 1.6 Hz, H-4′), 3.81 (3H, s, 4″-OCH$_3$). ^{13}C NMR (100 MHz, DMSO-d_6) (ppm): 162.3, 156.9, 154.4, 146.6, 139.2, 133.6, 131.8, 130.4, 128.6 × 2, 128.6, 122.6, 119.7, 116.2, 115.0, 114.2 × 2, 55.5. HRMS (ESI, *m/z*) calcd. for $C_{18}H_{16}N_2O_4S$ $(M+H)^+$ 357.0904, found 357.0900. Purity: 99% by HPLC (t_R = 2.343 min).

N-(2-(4-hydroxyphenyl)pyridin-3-yl)-4-methoxybenzenesulfonamide (HoAn13). White powder. Yield: 57%. M.p: 149.1–150.0 °C. ^{1}H NMR (400 MHz, DMSO-d_6) (ppm): 9.62 (1H, s, -NHSO$_2$-), 9.61 (1H, s, 4-OH), 8.41 (1H, dd, J_1 = 8.4 Hz, J_2 = 1.2 Hz, H-6′), 7.52 (2H, d, J = 9.2 Hz, H-2, H-6), 7.40 (1H, dd, J_1 = 8.0 Hz, J_2 = 1.6 Hz, H-4′), 7.35 (2H, d, J = 8.4 Hz, H-2″, H-6″), 7.22 (1H, dd, J_1 = 8.0 Hz, J_2 = 4.8 Hz, H-5′), 6.98 (2H, d, J = 8.8 Hz, H-3″,

H-5″), 6.73 (2H, d, J = 8.4 Hz, H-3, H-5), 3.82 (3H, s, 4″-OC$\underline{H}_3$). ^{13}C NMR (100 MHz, DMSO-d_6) (ppm): 162.3, 157.5, 154.7, 146.8, 134.3, 132.0, 130.4 × 2, 130.0, 128.8, 128.6 × 2, 121.8, 114.5 × 2, 114.2 × 2, 55.5. HRMS (ESI, *m/z*) calcd. for $C_{18}H_{16}N_2O_4S$ $(M+H)^+$ 357.0904, found 357.0904. Purity: 99% by HPLC (t_R = 2.276 min).

Procedure C for Synthesizing of N-(2-(4-aminophenyl)pyridin-3-yl)-4-methoxybenzenesulfonamide (HoAn17). **HoAn16** (100 mg, 0.259 mmol), iron powder (43 mg, 0.778 mmol) and NH_4Cl (138 mg, 2.59 mmol) was dissolved in ethanol/H_2O (3/1, v/v, 10 mL). The mixture was stirred under reflux at 100 °C for 3 h. After the reaction was finished, the iron powder was removed by filtering with diatomite, and the filtrate was removed under reduced pressure. The left mixture was extracted with EA/H_2O (2/1, v/v, 200 mL) for three times and then the organic layer was collected and concentrated to give the crude product. Further purified by silica gel column chromatography (PE: EA = 1: 1.5) could obtain the final yellow solid **HoAn17** (74 mg, 80%). M.p: 170.0–170.9 °C. ^{1}H NMR (400 MHz, DMSO-d_6) (ppm): 9.53 (1H, s, -N$\underline{H}$SO$_2$-), 8.36 (1H, d, J = 3.2 Hz, H-6′), 7.55 (2H, d, J = 8.8 Hz, H-2, H-6), 7.35 (1H, dd, J_1 = 8.0 Hz, J_2 = 1.2 Hz, H-4′), 7.28 (2H, d, J = 8.4 Hz, H-2″, H-6″), 7.14 (1H, dd, J_1 = 8.0 Hz, J_2 = 4.8 Hz, H-5′), 7.00 (2H, d, J = 8.8 Hz, H-3″, H-5″), 6.53 (2H, d, J = 8.8 Hz, H-3, H-5), 5.32 (2H, s, -N$\underline{H}_2$), 3.82 (3H, s, 4″-OC$\underline{H}_3$). ^{13}C NMR (100 MHz, DMSO-d_6) (ppm): 162.2, 154.9, 148.9, 146.6, 133.8, 132.1, 130.0 × 2, 129.6, 128.6 × 2, 125.2, 121.1, 114.2 × 2, 112.9 × 2, 55.6. HRMS (ESI, *m/z*) calcd. for $C_{18}H_{17}N_3O_3S$ $(M+H)^+$ 356.1063, found 356.1059. Purity: 95% by HPLC (t_R = 3.299 min).

Compound **HoAn19** was prepared with a similar procedure which described for the synthesis of **HoAn17**.

N-(2-(3-aminophenyl)pyridin-3-yl)-4-methoxybenzenesulfonamide (HoAn19). Yellow powder. Yield: 63%. M.p: 115.1–115.9 °C. ^{1}H NMR (400 MHz, DMSO-d_6) (ppm): 9.49 (1H, s, -N$\underline{H}$SO$_2$-), 8.38 (1H, dd, J_1 = 8.4 Hz, J_2 = 1.2 Hz, H-6′), 7.58 (2H, d, J = 8.8 Hz, H-2″, H-6″), 7.45 (1H, dd, J_1 = 8.0 Hz, J_2 = 1.2 Hz, H-4′), 7.25 (1H, dd, J_1 = 8.0 Hz, J_2 = 4.8 Hz, H-5′), 7.02-6.99 (3H, m, H-6, H-3″, H-5″), 6.67 (1H, s, H-2), 6.61-6.57 (2H, m, H-4, H-5), 5.08 (2H, s, -N$\underline{H}_2$), 3.82 (3H, s, 4″-OCH$_3$). ^{13}C NMR (100 MHz, DMSO-d_6) (ppm): 162.3, 154.5, 148.3, 146.2, 138.5, 132.5, 131.8, 130.4, 128.7 × 2, 128.1, 122.3, 116.6, 114.9, 114.2 × 2, 113.7, 55.6. HRMS (ESI, *m/z*) calcd. for $C_{18}H_{17}N_3O_3S$ $(M+H)^+$ 356.1063, found 356.1063. Purity: 95% by HPLC (t_R = 2.406 min).

Procedure D for Synthesizing of N-([2,4′-bipyridin]-3-yl)-4-methoxybenzenesulfonamide (HoAn25). 2-bromopyridin-3-amine (**1**) (500 mg, 2.89 mmol), pyridin-4-ylboronic acid (355 mg, 2.89 mmol), $Pd(PPh_3)_4$ (167 mg, 0.144 mmol) and K_2CO_3 (1.20 g, 8.67 mmol) was dissolved in dioxane/H_2O (2/1, v/v, 25 mL). The mixture was stirred under reflux at 120 °C for 12 h containing N_2 atmosphere. After cooling to room temperature, the solvent was concentrated and extracted with EA/H_2O (1/1, v/v, 500 mL) for three times. The organic layer was concentrated and the crude product was purified by silica gel column chromatography (PE: EA = 1: 2) to give a brown solid [2,4′-bipyridin]-3-amine (**2u**) (178 mg, 36%).

Compound **2u** (100 mg, 0.584 mmol), 4-methoxybenzenesulfonyl chloride (145 mg, 0.701 mmol), pyridine (0.5 mL) and DMAP (35 mg, 0.292 mmol) was dissolved in CH_2Cl_2 and stirred under reflux at 70 °C for 10 h. Then the reaction mixture was concentrated under reduced pressure, extracted with EA/H_2O (2/1, v/v, 150 mL) for three times. The organic layer was collected and removed, then the crude product was purified by silica gel column chromatography (PE: EA = 1: 2) to give a white solid **HoAn25** (109 mg, 55%). M.p: 176.5–177.4 °C. ^{1}H NMR (400 MHz, $CDCl_3$) (ppm): 8.53 (2H, d, J = 6.0 Hz, H-3, H-5), 8.46 (1H, dd, J_1 = 4.8 Hz, J_2 = 1.6 Hz, H-6′), 7.97 (1H, dd, J_1 = 8.4 Hz, J_2 = 1.6 Hz, H-4′), 7.57 (2H, d, J = 9.2 Hz, H-2″, H-6″), 7.33 (1H, dd, J_1 = 8.4 Hz, J_2 = 4.8 Hz, H-5′), 7.11 (2H, d, J = 6.0 Hz, H-2, H-6), 6.88 (2H, d, J = 9.2 Hz, H-3″, H-5″), 3.85 (3H, s, 4″-OCH$_3$). ^{13}C NMR (100 MHz, $CDCl_3$) (ppm): 163.5, 150.0 × 2, 149.1, 146.5, 144.8, 131.3, 131.2, 130.5, 129.1 × 2, 124.1, 123.3 × 2, 114.5 × 2, 55.7. HRMS (ESI, *m/z*) calcd. for $C_{17}H_{15}N_3O_3S$ $(M+H)^+$ 342.0907, found 342.0900. Purity: 98% by HPLC (t_R = 2.042 min).

Compounds **HoAn26** and **HoAn27** was prepared with a similar procedure which described for the synthesis of **HoAn25**.

N-([2,3′-bipyridin]-3-yl)-4-methoxybenzenesulfonamide (HoAn26). Yellow powder. Yield: 58%. M.p: 154.6–155.5 °C. ^{1}H NMR (400 MHz, $CDCl_3$) (ppm): 8.55 (1H, s, H-2), 8.46 (1H, d, J = 4.4 Hz, H-6), 8.39 (1H, s, H-4), 7.99 (1H, d, J = 8.0 Hz, H-6′), 7.55 (2H, d, J = 9.2 Hz, H-2″, H-6″), 7.53 (1H, d, J = 8.0 Hz, H-5), 7.32-7.29 (2H, m, H-4′, H-5′), 6.87 (2H, d, J = 8.8 Hz, H-3″, H-5″), 3.84 (3H, s, 4″-OCH$_3$). ^{13}C NMR (100 MHz, $CDCl_3$) (ppm): 163.4, 149.6, 149.1, 146.5, 136.5, 131.5, 131.3, 131.2, 130.5, 130.4, 129.1 × 2, 123.7, 123.6, 114.4 × 2, 55.7. HRMS (ESI, *m/z*) calcd. for $C_{17}H_{15}N_3O_3S$ $(M+H)^+$ 342.0907, found 342.0907. Purity: 97% by HPLC (t_R = 2.035 min).

4-methoxy-N-(2-(pyrimidin-5-yl)pyridin-3-yl)benzenesulfonamide (HoAn27). Yellowish powder. Yield: 69%. M.p: 164.7–165.6 °C. ^{1}H NMR (400 MHz, DMSO-d_6) (ppm): 10.08 (1H, s, -N$\underline{H}$SO$_2$-), 9.17 (1H, s, H-4), 8.88 (2H, s, H-2, H-6), 8.59 (1H, dd, J_1 = 4.8 Hz, J_2 = 1.6 Hz, H-6′), 7.49 (1H, dd, J_1 = 8.0 Hz, J_2 = 1.6 Hz, H-4′), 7.45-7.42 (3H, m, H-5′, H-2″, H-6″), 6.98 (2H, d, J = 9.2 Hz, H-3″, H-5″), 3.81 (3H, s, 4″-OCH$_3$). ^{13}C NMR (100 MHz, DMSO-d_6) (ppm): 162.5, 157.4, 156.2 × 2, 150.0, 148.1, 135.8, 132.1, 131.2, 130.7, 128.6 × 2, 124.2, 114.4 × 2, 55.6. HRMS (ESI, *m/z*) calcd. for $C_{16}H_{14}N_4O_3S$ $(M+H)^+$ 343.0859, found 343.0844. Purity: 97% by HPLC (t_R = 1.879 min).

Procedure E for Synthesizing of N-(2-(2,3-dimethoxyphenyl) pyridin-3-yl)-4-methoxy-N-((4-methoxyphenyl)sulfonyl)benzenesulfonamide (HoAn28). The intermediate 2-(2,3-dimethoxyphenyl)pyridin-3-amine (**2d**) was prepared with a similar procedure which described for the synthesis of the intermediate **2a** in **Procedure A** with a 58% yield.

Compound **2d** (100 mg, 0.434 mmol), 4-methoxybenzenesulfonyl chloride (269 mg, 1.30 mmol) and TEA (0.301 mL, 2.17 mmol) was dissolved in CH_2Cl_2, and the mixture was stirred under reflux at 68 °C for 12 h. After the reaction was completed, the solvent was removed and extracted with EA/H_2O (1/1, v/v, 200 mL) for three times. The EA layer was concentrated and purified by silica gel column chromatography (PE: EA = 2: 1) to obtain a yellow solid **HoAn28** (132 mg, 76%). M.p: 176.3–177.2 °C. ^{1}H NMR (400 MHz, $CDCl_3$) (ppm): 8.72 (1H, dd, J_1 = 4.4 Hz, J_2 = 1.6 Hz, H-6′), 7.73 (4H, d, J = 7.6 Hz, H-2" × 2, H-6" × 2), 7.37 (1H, dd, J_1 = 8.0 Hz, J_2 = 1.6 Hz, H-6), 7.29 (1H, dd, J_1 = 8.0 Hz, J_2 = 1.6 Hz, H-4), 7.24 (1H, dd, J_1 = 8.0 Hz, J_2 = 4.4 Hz, H-5′), 6.95 (1H, t, J = 7.6 Hz, H-5), 6.87-6.83 (5H, m, H-4′, H-3' × 2′, H-5" × 2), 3.88 (6H, s, 4″-OCH$_3$ × 2), 3.86 (3H, s, 3-OCH$_3$), 3.74 (3H, s, 2-OCH$_3$). ^{13}C NMR (100 MHz, $CDCl_3$) (ppm): 163.7 × 2, 158.9, 152.7, 149.7, 147.4, 139.4, 132.6, 131.5 × 2, 130.9, 130.3 × 2, 123.0, 122.4 × 4, 113.7 × 4, 112.8, 61.1, 55.6 × 2, 55.5. HRMS (ESI, *m/z*) calcd. for $C_{27}H_{26}N_2O_8S_2$ $(M+H)^+$ 571.1203, found 571.1203. Purity: 95% by HPLC (t_R = 7.342 min).

Compounds **HoAn29-HoAn31** was prepared with a similar procedure which described for the synthesis of **HoAn28**.

N-(2-(2,4-dimethoxyphenyl)pyridin-3-yl)-4-methoxy-N-((4-methoxyphenyl)sulfonyl)benzenesulfonamide (HoAn29). Yellow powder. Yield: 78%. M.p: 182.1–182.9 °C. ^{1}H NMR (400 MHz, $CDCl_3$) (ppm): 8.73 (1H, dd, J_1 = 4.8 Hz, J_2 = 1.6 Hz, H-6′), 7.69-7.65 (5H, m, H-6, H-2" × 2, H-6" × 2), 7.29 (1H, dd, J_1 = 8.4 Hz, J_2 = 1.6 Hz, H-4′), 7.21 (1H, dd, J_1 = 8.0 Hz, J_2 = 4.4 Hz, H-5′), 6.85 (4H, d, J = 8.8 Hz, H-3" × 2, H-5" × 2), 6.43 (1H, dd, J_1 = 8.4 Hz, J_2 = 2.4 Hz, H-5), 6.31 (1H, d, J = 2.0 Hz, H-3), 3.89 (6H, s, 4″-OCH$_3$ × 2), 3.83 (3H, s, 4-OCH$_3$), 3.62 (3H, s, 2-OCH$_3$). ^{13}C NMR (100 MHz, $CDCl_3$) (ppm): 163.7 × 2, 161.2, 158.4, 149.9, 139.4, 131.3 × 5, 131.1, 130.5 × 2, 122.1 × 2, 113.7 × 5, 103.6, 99.0, 55.6 × 2, 55.4, 55.3. HRMS (ESI, *m/z*)

calcd. for $C_{27}H_{26}N_2O_8S_2$ $(M+H)^+$ 571.1203, found 571.1185. Purity: 99% by HPLC (t_R = 5.687 min).

N-(2-(2,5-dimethoxyphenyl)pyridin-3-yl)-4-methoxy-N-((4-methoxyphenyl)sulfonyl)benzenesulfonamide (HoAn30). Yellow powder. Yield: 70%. M.p: 154.1–155.0 °C. ^{1}H NMR (400 MHz, DMSO-d_6) (ppm): 8.70 (1H, dd, J_1 = 4.8 Hz, J_2 = 1.6 Hz, H-6′), 7.64-7.53 (4H, m, H-2" × 2, H-6" × 2), 7.43 (1H, dd, J_1 = 8.0 Hz, J_2 = 4.8 Hz, H-5′), 7.23 (1H, dd, J_1 = 8.0 Hz, J_2 = 1.6 Hz, H-3), 7.19 (1H, d, J = 2.8 Hz, H-6), 7.04 (4H, d, J = 8.8 Hz, H-3" × 2, H-5" × 2), 6.92-6.84 (2H, m, H-4, H-4′), 3.88 (6H, s, 4″-OCH_3 × 2), 3.68 (3H, s, 5-OCH_3), 3.53 (3H, s, 2-OCH_3). ^{13}C NMR (100 MHz, DMSO-d_6) (ppm): 163.7 × 2, 157.9, 152.1, 151.3, 150.1, 138.9, 130.8, 130.0, 129.2 × 4, 127.0, 123.1 × 2, 115.6, 114.8, 114.2 × 4, 112.6, 55.9 × 2, 55.6, 55.4. HRMS (ESI, *m/z*) calcd. for $C_{27}H_{26}N_2O_8S_2$ $(M+H)^+$ 571.1203, found 571.1177. Purity: 95% by HPLC (t_R = 5.695 min).

N-(2-(benzo[d] [1,3]dioxol-5-yl)pyridin-3-yl)-4-methoxy-N-((4-methoxyphenyl)sulfonyl)benzenesulfonamide (HoAn31). Yellow powder. Yield: 77%. M.p: 188.8–189.7 °C. ^{1}H NMR (400 MHz, $CDCl_3$) (ppm): 8.70 (1H, dd, J_1 = 4.4 Hz, J_2 = 1.6 Hz, H-6′), 7.72 (4H, d, J = 9.2 Hz, H-2" × 2, H-6" × 2), 7.31-7.26 (2H, m, H-5, H-6), 7.22 (1H, dd, J_1 = 8.0 Hz, J_2 = 4.4 Hz, H-5′), 7.09 (1H, d, J = 2.0 Hz, H-2), 6.88 (4H, d, J = 8.8 Hz, H-3" × 2, H-5" × 2), 6.70 (1H, d, J = 8.4 Hz, H-4′), 5.93 (2H, s, -OCH_2O-), 3.90 (6H, s, 4″-OCH_3 × 2). ^{13}C NMR (100 MHz, $CDCl_3$) (ppm): 163.9 × 2, 159.5, 150.6, 148.0, 147.3, 139.9, 131.4 × 4, 130.5 × 2, 130.2, 124.0 × 2, 122.2, 113.8 × 4, 110.1, 107.9, 101.1, 55.7 × 2. HRMS (ESI, *m/z*) calcd. for $C_{26}H_{22}N_2O_8S_2$ $(M+H)^+$ 555.0890, found 555.0880. Purity: 98% by HPLC (t_R = 7.238 min).

Procedure F for Synthesizing of N-(2-(4-cyano-3-fluorophenyl)pyridin-3-yl)-4-methoxybenzenesulfonamide (HoAn32). The intermediate 4-(3-aminopyridin-2-yl)-2-fluorobenzonitrile (**2t**) was prepared with a similar procedure which described for the synthesis of the intermediate **2a** in **Procedure A** with a 70% yield.

Compound **2t** (100 mg, 0.469 mmol), DMAP (28 mg, 0.234 mmol) and pyridine (0.5 mL) was dissolved in CH_2Cl_2, and then 4-methoxybenzenesulfonyl chloride (116 mg, 0.562 mmol) was added slowly within 5 min. The reaction mixture was stirred under reflux at 65 °C for 12 h. Till the reaction finished, the mixture was concentrated and extracted with EA/H_2O (2/1, v/v, 250 mL) for three times. EA was removed under reduced pressure and the crude product was separated by silica gel column chromatography (PE: EA = 4: 1) to obtain a white solid **HoAn32** (79 mg, 44%). M.p: 158.6–159.5 °C. ^{1}H NMR (400 MHz, DMSO-d_6) (ppm): 9.95 (1H, s, -N$\underline{H}SO_2$-), 8.56 (1H, dd, J_1 = 8.8 Hz, J_2 = 1.6 Hz, H-6′), 7.90 (1H, t, J = 7.2 Hz, H-6), 7.55 (1H, dd, J_1 = 8.0 Hz, J_2 = 1.6 Hz, H-5), 7.51-7.43 (3H, m, H-2, H-4′, H-5′), 7.40 (2H, d, J = 8.8 Hz, H-2″, H-6″), 6.96 (2H, d, J = 9.2 Hz, H-3″, H-5″), 3.82 (3H, s, 4″-$OC\underline{H}_3$). ^{13}C NMR (100 MHz, DMSO-d_6) (ppm): 162.4, 160.6, 152.2, 147.8, 145.6, 145.5, 136.5, 133.2, 131.1, 130.7, 128.6 × 2, 126.0, 124.4, 116.8, 114.2 × 2, 113.9, 55.6. HRMS (ESI, *m/z*) calcd. for $C_{19}H_{14}FN_3O_3S$ $(M+H)^+$ 384.0813, found 384.0816. Purity: 98% by HPLC (t_R = 6.219 min).

Compounds **HoAn33-HoAn40** was prepared with a similar procedure which described for the synthesis of **HoAn32**. (The reagent 4-methoxybenzenesulfonyl chloride was replaced by different substituted benzensulfonyl chloride.)

N-(2-(4-cyano-3-fluorophenyl)pyridin-3-yl)-4-methylbenzenesulfonamide (HoAn33). Yellowish powder. Yield: 40%. M.p: 176.6–177.5 °C. ^{1}H NMR (400 MHz, $CDCl_3$) (ppm): 8.48 (1H, dd, J_1 = 4.8 Hz, J_2 = 1.6 Hz, H-6′), 7.99 (1H, dd, J_1 = 8.0 Hz, J_2 = 1.2 Hz, H-6), 7.59 (1H, t, J = 7.2 Hz, H-5), 7.46 (2H, d, J = 8.0 Hz, H-2″, H-6″), 7.37 (1H, dd, J_1 = 8.4 Hz, J_2 = 4.8 Hz, H-2), 7.24 (2H, d, J = 8.8 Hz, H-3″, H-5″), 7.12 (1H, dd, J_1 = 8.0 Hz, J_2 = 1.6 Hz, H-5′), 6.86 (1H, dd, J_1 = 9.2 Hz, J_2 = 1.2 Hz, H-4′), 6.74 (1H, s, -N$\underline{H}SO_2$-), 2.44 (3H, s, 4″-$C\underline{H}_3$). ^{13}C NMR (100 MHz, $CDCl_3$) (ppm): 164.3, 161.7, 149.3, 146.9, 145.0, 135.6, 133.7, 132.4, 130.8, 130.0 × 2, 126.9 × 2, 125.0, 124.4, 117.2, 117.0, 113.4, 21.5. HRMS (ESI, *m/z*) calcd. for $C_{19}H_{14}FN_3O_2S$ $(M+H)^+$ 368.0864, found 368.0868. Purity: 99% by HPLC (t_R = 3.753 min).

4-chloro-N-(2-(4-cyano-3-fluorophenyl)pyridin-3-yl)benzenesulfonamide (HoAn34). Grey-white powder. Yield: 38%. M.p: 180.9–181.8 °C. ^{1}H NMR (400 MHz, $CDCl_3$) (ppm): 8.52 (1H, d, J = 4.0 Hz, H-6′), 7.94 (1H, d, J = 8.0 Hz, H-6), 7.66 (1H, t, J = 7.2 Hz, H-5), 7.55 (2H, d, J = 8.4 Hz, H-2″, H-6″), 7.44 (2H, d, J = 8.4 Hz, H-3″, H-5″), 7.38 (1H, dd, J_1 = 8.0 Hz, J_2 = 4.8 Hz, H-2), 7.17 (1H, d, J = 8.0 Hz, H-5′), 7.02 (1H, d, J = 9.6 Hz, H-4′), 6.59 (1H, s, -N$\underline{H}SO_2$-). ^{13}C NMR (100 MHz, $CDCl_3$) (ppm): 170.2, 153.1, 147.3, 140.6, 137.1, 133.9, 132.1, 130.4, 129.7 × 2, 128.4 × 2, 125.0, 124.9, 124.5, 117.2, 116.9, 113.2. HRMS (ESI, *m/z*) calcd. for $C_{18}H_{11}ClFN_3O_2S$ $(M+H)^+$ 388.0317, found 388.0310. Purity: 99% by HPLC (t_R = 3.465 min).

4-bromo-N-(2-(4-cyano-3-fluorophenyl)pyridin-3-yl)benzenesulfonamide (HoAn35). Grey-white powder. Yield: 53%. M.p: 192.8–193.6 °C. ^{1}H NMR (400 MHz, DMSO-d_6) (ppm): 10.28 (1H, s, -N$\underline{H}SO_2$-), 8.60 (1H, dd, J_1 = 4.8 Hz, J_2 = 1.6 Hz, H-6′), 7.89 (1H, t, J = 7.2 Hz, H-5), 7.65 (2H, d, J = 8.4 Hz, H-2″, H-6″), 7.57 (1H, dd, J_1 = 8.0 Hz, J_2 = 1.2 Hz, H-2), 7.52-7.46 (3H, m, H-6, H-4′, H-5′), 7.38 (2H, d, J = 8.4 Hz, H-3″, H-5″). ^{13}C NMR (100 MHz, DMSO-d_6) (ppm): 163.1, 160.6, 152.7, 148.3, 145.5, 145.4, 138.9, 137.3, 133.3, 132.2, 130.2, 128.3, 126.8, 126.1, 124.5, 116.8, 116.6, 113.8. HRMS (ESI, *m/z*) calcd. for $C_{18}H_{11}BrFN_3O_2S$ $(M-H)^-$ 429.9667, found 429.9682. Purity: 97% by HPLC (t_R = 3.621 min).

N-(2-(4-cyano-3-fluorophenyl)pyridin-3-yl)-4-(trifluoromethyl)benzenesulfonamide (HoAn36). Yellowish powder. Yield: 68%. M.p: 183.7–184.6 °C. ^{1}H NMR (400 MHz, $CDCl_3$) (ppm): 8.54 (1H, d, J = 4.0 Hz, H-6′), 7.93 (1H, d, J = 8.0 Hz, H-6), 7.74 (4H, m, H-2″, H-3″, H-5″, H-6″), 7.63 (1H, t, J = 7.2 Hz, H-5), 7.39 (1H, dd, J_1 = 8.0 Hz, J_2 = 4.8 Hz, H-2), 7.16 (1H, d, J = 8.0 Hz, H-5′), 6.99 (1H, d, J = 9.2 Hz, H-4′), 6.80 (1H, s, -N$\underline{H}SO_2$-). ^{13}C NMR (100 MHz, $CDCl_3$) (ppm): 164.2, 161.6, 149.6, 147.5, 143.8, 143.7, 142.2, 133.9, 132.5, 130.1, 127.5 × 2, 126.6, 126.5, 125.0, 124.5, 117.1, 116.9, 113.2. HRMS (ESI, *m/z*) calcd. for $C_{19}H_{11}F_4N_3O_2S$ $(M-H)^-$ 420.0435, found 420.0456. Purity: 95% by HPLC (t_R = 10.878 min).

N-(2-(4-cyano-3-fluorophenyl)pyridin-3-yl)benzenesulfonamide (HoAn37). White powder. Yield: 60%. M.p: 188.8–189.7 °C. ^{1}H NMR (400 MHz, DMSO-d_6) (ppm): 10.14 (1H, s, -N$\underline{H}SO_2$-), 8.56 (1H, dd, J_1 = 4.8 Hz, J_2 = 1.2 Hz, H-6′), 7.91 (1H, t, J = 7.2 Hz, H-6), 7.64-7.60 (1H, m, 4″), 7.53-7.42 (8H, m, H-2, H-5, H-4′, H-5′, H-2″, H-3″, H-5″, H-6″). ^{13}C NMR (100 MHz, DMSO-d_6) (ppm): 163.1, 160.6, 152.2, 147.9, 145.6, 145.5, 136.2, 133.3, 132.8, 130.6, 129.2 × 2, 126.3 × 2, 126.0, 124.4, 116.8, 113.9. HRMS (ESI, *m/z*) calcd. for $C_{18}H_{12}FN_3O_2S$ $(M+H)^+$ 354.0707, found 354.0716. Purity: 96% by HPLC (t_R = 3.158 min).

N-(2-(4-cyano-3-fluorophenyl)pyridin-3-yl)naphthalene-2-sulfonamide (HoAn38). White powder. Yield: 51%. M.p: 168.9–169.8 °C. ^{1}H NMR (400 MHz, DMSO-d_6) (ppm): 10.25 (1H, s, -N$\underline{H}SO_2$-), 8.57 (1H, dd, J_1 = 4.8 Hz, J_2 = 1.6 Hz, H-6′), 8.09 (1H, s, H-2″), 8.04-7.97 (3H, m, H-6, H-5″, H-6″), 7.73-7.63 (3H, m, H-5, H-a, H-d), 7.59 (1H, dd, J_1 = 8.0 Hz, J_2 = 1.2 Hz, H-2), 7.52 (1H, dd, J_1 = 8.8 Hz, J_2 = 1.6 Hz, H-b), 7.47-7.40 (3H, m, H-c, H-4′, H-5′). ^{13}C NMR (100 MHz, DMSO-d_6) (ppm): 162.9, 160.4, 152.6, 148.2, 137.3, 136.7, 134.1, 133.0, 131.4, 130.4, 129.3, 129.1, 129.0, 127.7, 127.6, 127.3, 125.9, 124.4, 121.7, 116.6, 116.4, 113.7. HRMS (ESI, *m/z*) calcd. for $C_{22}H_{14}FN_3O_2S$ $(M-H)^-$ 402.0718, found 402.0744. Purity: 99% by HPLC (t_R = 4.240 min).

N-(2-(4-cyano-3-fluorophenyl)pyridin-3-yl)-4-(trifluoromethoxy)benzenesulfonamide (HoAn39). Yellowish powder. Yield: 35%. M.p: 162.6–163.5 °C. ^{1}H NMR (400 MHz, $CDCl_3$) (ppm): 8.53 (1H, d, J = 3.6 Hz, H-6′), 7.94 (1H, d, J = 7.6 Hz, H-6), 7.67 (2H, d, J = 8.8 Hz, H-2″, H-6″), 7.63 (1H, d, J = 7.2 Hz, H-5), 7.38 (1H, dd, J_1 = 8.0 Hz, J_2 = 4.8 Hz, H-2), 7.28 (2H, d, J = 8.4 Hz, H-3″, H-5″), 7.16 (1H, d, J = 7.6 Hz, H-5′), 7.01 (1H, d, J = 9.2 Hz, H-4′), 6.77 (1H, s,

-NHSO$_2$-). ^{13}C NMR (100 MHz, $CDCl_3$) (ppm): 164.3, 161.7, 152.8, 149.4, 147.4, 143.9, 143.8, 136.9, 133.9, 132.3, 130.3, 129.2 × 2, 125.0, 124.5, 121.0, 117.1, 116.9, 113.2. HRMS (ESI, *m/z*) calcd. for $C_{19}H_{11}F_4N_3O_3S$ $(M-H)^-$ 436.0384, found 436.0403. Purity: 97% by HPLC (t_R = 3.074 min).

N-(2-(4-cyano-3-fluorophenyl)pyridin-3-yl)-3,4-dimethoxybenzenesulfonamide (HoAn40). Yellowish powder. Yield: 66%. M.p: 141.5–142.3 °C. ^{1}H NMR (400 MHz, DMSO-d_6) (ppm): 9.92 (1H, s, -NHSO$_2$-), 8.57 (1H, d, J = 3.6 Hz, H-6′), 7.88 (1H, t, J = 7.2 Hz, H-6), 7.60 (1H, d, J = 8.0 Hz, H-5), 7.49-7.44 (3H, m, H-2, H-2″, H-6″), 6.99-6.91 (3H, m, H-4′, H-5′, H-5″), 3.82 (3H, s, 3″-OCH$_3$), 3.67 (3H, s, 4″-OCH$_3$). ^{13}C NMR (100 MHz, DMSO-d_6) (ppm): 163.0, 160.5, 152.3, 148.4, 147.9, 145.4, 145.3, 137.0, 133.0, 130.7, 126.0, 124.4, 120.3, 116.7, 116.5, 113.9, 110.7, 108.5, 55.7, 55.3. HRMS (ESI, *m/z*) calcd. for $C_{20}H_{16}FN_3O_4S$ $(M-H)^-$ 412.0773, found 412.0794. Purity: 98% by HPLC (t_R = 2.832 min).

4.2. Biology

4.2.1. Cell lines and culture

The human cancer cell lines (MCF-7, SK-HEP-1, RKO, PLC/PRF/5, HCC-LM3, BT474, SK-BR-3, SW620, SW480, A549, H460, PANC-1 and SGC-7901) were purchased from Cell Bank of the Chinese Academy of Science (Shanghai, China), and the HUVEC cell line was purchased from ATCC (Washington, DC, USA). Cell lines including MCF-7, SK-HEP-1, PLC/PRF/5, HCC-LM3, SK-BR-3, A549, PANC-1 and HUVEC were cultivated in DMEM medium (CR-12800-S, Zhejiang Senrui Biological Technology Co., Ltd, Huzhou, China). Cell lines including BT474, RKO, SW620, SW480, H460 and SGC-7901 were maintained in RPMI 1640 medium (CR-31800-S, Zhejiang Senrui Biological Technology Co., Ltd, Huzhou, China). The medium used in all cell lines were supplemented with 10% (v/v) fetal bovine serum (FBS), 100 μg/mL streptomycin, and 100 U/mL penicillin. All cell lines were cultivated at 37 °C in a humidified atmosphere with 5% CO_2.

4.2.2. Antibodies and reagents

Primary antibodies including anti-β-actin (4970, 1:1000), anti-Cdc2 (77055, 1:1000), anti-Cyclin B1 (4138, 1:1000), anti-Bax (2772, 1:1000) and anti-Cleaved PARP (9541, 1:1000) were purchased from Cell Signaling Technology (Shanghai, China), and anti-β-tubulin antibody (ET1602-4, 1:2000) was purchased from Hangzhou HuaAn Biotechnology Co., Ltd (Zhejiang, China). Second antibodies including the goat anti-rabbit IgG (H+L) highly cross-adsorbed secondary antibody/Alexa Fluor Plus 594 (A32740) was purchased from Invitrogen (Camarillo, CA, USA) and Peroxidase AffiniPure Goat Anti-Rabbit IgG (H+L) (111-035-003, 1:5000) was purchased from Jackson ImmunoResearch (Pennsylvania, USA). The cell cycle staining kit (CCS012) was purchased from Multi Sciences (Hangzhou, China) and FITC Annexin V apoptosis detection kit (556547) was purchased from BD Biosciences (New Jersey, USA). Reactive Oxygen Species assay kit (S0033S) was purchased from Beyotime (Shanghai, China). A commercial kit (#BK004P) used for the tubulin polymerization assay was purchased from Cytoskeleton (Danvers, MA, USA). 3-(4,5-dimethylthiazol-2-yl)-5-(3-carboxymethoxyphenyl)-2-(4-sulfophenyl)-2H-tetrazolium (MTS, G111A) was purchased from Promega (Madison, WI, USA). Honokiol (CSN19405, purity ≥ 99.9%) and **ABT-751** (CSN16987, purity ≥ 99.9%) were purchased from CSNpharm (Shanghai, China). Corn oil (C116023) was obtained from aladdin (Shanghai, China). *N*,*N*′-ethylene-bis(iodoacetamide) (EBI, E917500) was obtained from TRC (Toronto, Canada). Stock solution (20 mM) of compounds was prepared with dimethyl sulfoxide (DMSO) (Sigma-Aldrich, St. Louis, MO) and freshly diluted with cell culture medium before use.

4.2.3. MTS assay

The *in vitro* antiproliferative effect of compounds was determined by the MTS assay. Briefly, cells grown in the logarithmic phase were seeded into 96-well plates (5×10^3–6×10^3 cells per well, depending on the growth rate of the cell line) for 24 h. After that, fresh medium (100 μl) containing the test compound at a certain concentration was added to each well and incubated for 72 h in five replicates. Then the old medium was replaced by fresh medium (100 μl) containing 10% MTS and the cells were incubated in dark at 37 °C for at least 30 min. The optical density value at 490 nm of each well was recorded in BioTek Synergy H4 microplate Reader (Vermont, USA). The cytotoxic effect of test compound was expressed as the inhibitory rate or IC_{50} value, which was calculated by the nonlinear regression analysis using GraphPad Prism 7.0 (GraphPad Software, San Diego, CA).

4.2.4. In vitro tubulin polymerization assay

The tubulin polymerization assay was performed according to the procedures provided by a commercial kit (#BK004P) purchased from Cytoskeleton (Danvers, MA, USA) with appropriate modification. Briefly, porcine tubulin protein (4 mg, >97% pure) was resuspended with 400 μL ice-cold general tubulin buffer (80 mM PIPES, 2.0 mM $MgCl_2$, 0.5 mM EGTA, pH = 6.9) to be tubulin stock solution (10 mg/mL). Then, 176 μL tubulin stock solution was diluted with 264 μL ice-cold general tubulin buffer and then added 4 μL GTP stock solution (100 mM) to be tubulin reaction mix (4 mg/mL). Meanwhile, 5 μL of the 2 mM test compound (**HoAn32**, **ABT-751**, paclitaxel and DMSO) stock solution was diluted with 95 μL of room temperature general tubulin buffer to form a solution with a concentration of 100 μM. Half area 96-well plate was pre-warmed in Synergy H4 microplate reader (BioTek, Winooski, Vermont, USA) at 37 °C for 30 min, and then 10 μL of the test compounds (100 μM) was added into the wells of the pre-warmed plate and incubated for another 5 min at 37 °C before detecting the tubulin polymerization reaction. After that, pre-cooled tubulin reaction mix was added into the corresponding wells (100 μL per well) immediately and the absorbance was detected by Synergy H4 microplate reader at 340 nm at 37 °C every 1 min for 60 min.

4.2.5. EBI competition assay

SW620 cells were seeded to 6-well plates (5×10^5 cells per well). Firstly, the cells were incubated with DMSO, **HoAn32** (10, 20 and 40 μM) and **ABT-751** (20 and 40 μM) for 2 h and then the cells were treated with EBI (100 μM) for 2 h. The cells were harvest and treatment with 1 × loading buffer (50 mM Tris-HCl PH = 6.8, SDS 2%, bromophenol blue 0.1%, glycerol 10%, DTT 1.5%) to prepare the cell extracts for western blot analysis. The next processes were similar to the steps described in chapter *4.2.9 Western Blot Assay* section, in which anti-*β*-tubulin antibody was used as primary antibody.

4.2.6. Immunofluorescence microscopy

RKO cells were seeded to 6-well plates (2.5×10^5 cells per well) with glass coverslips and incubated overnight. The cells were treated with DMSO, **HoAn32** (0.5 μM and 1 μM), **ABT-751** (1 μM) and paclitaxel (1 μM) and incubated for 24 h. Then the cells were washed with PBS for three times and fixed with pre-cooled methanol for 10 min. After permeabilization with 0.25% Triton X-100 for 10 min, the cells were washed with PBS for three times and blocked in 1% bovine serum albumin (BSA) at 4 °C overnight. The cells were incubated with rabbit anti-β-tubulin primary antibody containing 1% BSA (v/v, 1: 100) at room temperature for 2 h and washed with PBS for three times. After that, the cells were incubated with goat anti-rabbit IgG (H+L) highly cross-adsorbed secondary antibody/Alexa Fluor Plus 594 containing 1% BSA (v/v, 1:

500) at room temperature for 1 h and washed with PBS for three times. 4,6-diamidino-2-phenylindole (DAPI) (Thermo Fisher Scientific) was added and keep in dark for 1 h. Finally, fluorescence images of the cells were recorded on BX53 Upright Microscope (Olympus, Japan).

4.2.7. Cell cycle analysis

RKO, SW620 and PANC-1 cells were seeded into 6-well plates (4×10^5—5×10^5 cells per well) and incubated for 24 h. Subsequently, the cells were treated with DMSO, **HoAn32** (0.5 and 1 μM) and **ABT-751** (1 μM) for another 24 h. Then the cells were harvested by centrifugation and washed with PBS for three times, ice-cold 75% ethanol was added to fix cells at 4 °C overnight. After that, ethanol was removed and the cells were resuspended with ice-cold PBS, and then RNase A and the DNA staining solution propidium iodide (PI) (Multi Sciences, China) was added and keep the cells in the darkness at 37 °C for 30 min before detection. Finally, the cell cycle distribution was detected by a FACS Calibur flow cytometer (Bectone Dickinson, San Jose, CA, USA).

4.2.8. Cell apoptosis analysis

RKO and SW620 cells were seeded into 6-well plates (4×10^5—5×10^5 cells per well) and treatment with DMSO, **HoAn32** (0.5 and 1 μM) or **ABT-751** (1 μM) for 24 h. After incubation, the cells were harvested and washed with PBS for three times. Then, 100 μL of the mixture of Annexin V/FITC (BD Biosciences, USA) and PI in binding buffer (v/v, 5: 5: 100) was added and keep in the darkness at 37 °C for 30 min. Before detection, another 300 μL binding buffer was added into the sample and then apoptosis was analyzed by a FACS Calibur flow cytometer (Bectone Dickinson, San Jose, CA, USA).

4.2.9. Clonogenic assay

RKO or SW620 cells were embedded at a density of 1000 cells per well in 6-well plates overnight and then treated with DMSO、**HoAn32** (0.125 μM、0.25 μM、0.5 μM and 1 μM) and **ABT-751**(1 μM) for another 24 h. After that, the culture medium was replaced with fresh culture medium and the cells were continue to grow for another 10 days until analysis. After this stage, the culture medium was removed and washed with 1 × PBS for twice. Then, the cells were fixed with methanol for 15 min, and stained with 0.1% crystal violet for another 30 min. Finally, the cells were washed with water, dried and then photographed for visualization. More than 50 cells per colony were counted.

4.2.10. Measurement of intracellular ROS generation

Peroxide-sensitive fluorescent probe DCFH-DA was used for detecting intracellular ROS generation. In brief, cells were seeded into 6-well plates (5×10^5 cells per well) and incubated with DMSO、**HoAn32** (0.25 μM and 0.5 μM) and **ABT-751** (0.5 μM) for 24 h. Then the culture medium was replaced by 1 mL serum-free medium containing 5 μM DCFH-DA (1: 2000) and incubated for another 30 min at 37 °C. After that, DCFH-DA was washed with serum-free medium for twice. Then the cells were harvested, centrifugated and washed with PBS for twice. Finally, the samples were analyzed by a FACS Calibur flow cytometer (Bectone Dickinson, San Jose, CA, USA) at an excitation wavelength of 488 nm and an emission wavelength of 525 nm.

4.2.11. Western blot analysis

Cells were seeded into 6-well plates (4×10^5—5×10^5 cells per well) and incubated with DMSO, **HoAn32** (0.5 and 1 μM) and **ABT-751** (1 μM) for 24 h. After incubation, cells were washed with ice-cold PBS and the protein extracts were prepared in 1 × loading buffer (50 mM Tris-HCl PH = 6.8, SDS 2%, bromophenol blue 0.1%, glycerol 10%, DTT 1.5%). Then, the protein extracts were boiled for 15 min, sonicated, run in 8%—15% SDS-PAGE gels, transferred to polyvinylidene fluoride (PVDF) membranes (Beyotime, China) and blocked with 5% non-fat milk (dissolved in 1 × TBST). After that, the membranes were incubated with corresponding primary antibodies at 4 °C overnight, washed with 1 × TBST (TBS with 0.1% Tween-20) for three times, followed by incubating with horseradish peroxidase (HRP)-conjugated secondary antibody at room temperature for 2 h and washed with 1 × TBST for three times again. Finally, the immunoreactivity of the membranes was visualized by using a LAS-4000mini Luminescent Imaging Analyzer (Fujifilm, Japan) with an enhanced chemiluminescence kit (Beyotime, China) for HRP.

4.2.12. Molecular modeling

The crystal structure of tubulin in complex with **ABT-751** was downloaded from the Protein Data Bank (PDB codes: 3HKC, http://www.rcsb.org). The whole docking process took place in LeDock software. Briefly, molecular **HoAn32** was prepared in ChemBio3D Ultra 14.0 and optimized to obtain the lowest energy conformer. The protein structure was prepared in Lepro module. After extracting the ligand, hydrogen atoms were added to the crystal and then the charges were added to biopolymer by the CHARMm force field. Finally, the docking studies of **HoAn32** with the prepared protein occurred in Ledock module with the default settings. 6 poses were exported for the next analysis. The structural images were produced by PyMOL software.

4.2.13. Wound healing assays

HUVEC cells were seeded in 6-well plates at a density of 1×10^6 cells per well for 24 h. After producing scratches by using 200 μL pipette tips, the wounds were washed twice with 1 × PBS to remove nonadherent cell debris. Then, the cells were incubated with 0, 0.5 μM, and 1 μM of **HoAn32** or 1 μM of **ABT-751** for 24 h. Cells which migrated across the wound area were photographed through inverted microscopy (Primovert, ZEISS) at 0 and 24 h.

4.2.14. In vivo antitumor efficacy of HoAn32 in the SW620 colon cancer xenograft model

All the animal experimental procedures performed in accordance with the animal experiment guidelines of the Animal Care and Welfare Committee of Zhejiang University. The Five to six-week-old male athymic nude mice were purchased from Shanghai Laboratory Animal Center, CAS (SLACCAS) and fed under pathogen-free condition for one week before use. A total of 5×10^6 SW620 cells containing 125 μL PBS were subcutaneously inoculated into the right armpit of mice. When the tumor volumes reached about 100 mm^3, mice were randomized into vehicle or treatment groups (n = 6). **HoAn32** and **ABT-751** were dissolved in a 1:9 ratio of DMSO: corn oil mixed solution to produce desired concentrations. The vehicle control solution was prepared with equal parts of DMSO and corn oil only. Then, the mice were treatment with 100 μL **HoAn32** (p.o., 25 mg/kg, per 2 days), **ABT-751** (p.o., 25 mg/kg, per 2 days) or vehicle solution (p.o., per 2 days) for 20 days. Tumor volume and body weights were measured with Vernier calipers every 2 days after the start of drug administration. At the end of the experiment, the mice were sacrificed and the tumor bulks were peeled off for weighing. The data was dealt with by the following formula: tumor volume = L (length) × W^2 (width)/2; The ratio of inhibition of tumor (%) = (1 - tumor weight of treated group/tumor weight of vehicle group) × 100%.

4.2.15. H&E staining

The H&E staining experiences were conducted at Hangzhou HuaAn Biotechnology Co., Ltd (Hangzhou, China). The major organs

(heart, liver, spleen, lung and kidney) were isolated from nude mice, and then fixed in 4% paraformaldehyde, dehydration and embedded in paraffin using tissue embedding machine. The tissues were sectioned in the vertical plane into 4 μm-thick. Afterwards, the sections were dewaxing and staining with Mayer hematoxylin stain solution for 5 min following by eosin-phloxine solution for 2 min, and then dehydrated and mounted with neutral resin. Finally, the tissue morphology was observed under a microscope (NIKON ECLIPSE 80i).

4.2.16. Statistical analysis

Data were presented as mean ± SD (standard deviations). The statistical significance was evaluated by one-way ANOVA using GraphPad Prism 7.0 (GraphPad Software, Inc., San Diego, CA), comparing the tested groups to the control group. $P < 0.05$ was considered statistically significant.

Author contributions

The manuscript was written through contributions of all authors. All authors have given approval to the final version of the manuscript.

Declaration of competing interest

The authors declare that they have no known competing financial interests or personal relationships that could have appeared to influence the work reported in this paper.

Acknowledgements

This study was supported by the China State Key Research, Grant No. 2016YEF0200503 and the National Natural Science Foundation of China (No. 21532005) as well as the National Natural Science Foundation of China (No. 81761138047).

Appendix A. Supplementary data

Supplementary data to this article can be found online at https://doi.org/10.1016/j.ejmech.2020.113117.

References

[1] C. Delandre, R. Amikura, A.W. Moore, Microtubule nucleation and organization in dendrites, Cell Cycle 15 (2016) 1685–1692, https://doi.org/10.1080/15384101.2016.1172158.
[2] L.R. Vega, F. Solomon, Microtubule function in morphological differentiation: growth zones and growth cones, Cell 89 (1997) 825–828, https://doi.org/10.1016/s0092-8674(00)80266-4.
[3] T.J. Mitchison, Microtubule dynamics and kinetochore function in mitosis, Annu. Rev. Cell Biol. 4 (1988) 527–549, https://doi.org/10.1146/annurev.cb.04.110188.002523.
[4] T. Hohmann, F. Dehghani, The cytoskeleton-A complex interacting meshwork, Cells 8 (2019), https://doi.org/10.3390/cells8040362.
[5] A. Melkov, U. Abdu, Regulation of long-distance transport of mitochondria along microtubules, Cell. Mol. Life Sci. 75 (2018) 163–176, https://doi.org/10.1007/s00018-017-2590-1.
[6] L. Cirillo, M. Gotta, P. Meraldi, The elephant in the room: the role of microtubules in cancer, Adv. Exp. Med. Biol. 1002 (2017) 93–124, https://doi.org/10.1007/978-3-319-57127-0_5.
[7] E. Pasquier, M. Kavallaris, Microtubules: a dynamic target in cancer therapy, IUBMB Life 60 (2008) 165–170, https://doi.org/10.1002/iub.25.
[8] C.H. Yang, S.B. Horwitz, Taxol((R)): the first microtubule stabilizing agent, Int. J. Mol. Sci. 18 (2017), https://doi.org/10.3390/ijms18081733.
[9] C.D. Churchill, M. Klobukowski, J.A. Tuszynski, Analysis of the binding mode of laulimalide to microtubules: establishing a laulimalide-tubulin pharmacophore, J. Biomol. Struct. Dyn. 34 (2016) 1455–1469, https://doi.org/10.1080/07391102.2015.1078115.
[10] D.L. Sackett, J.K. Varma, Molecular mechanism of colchicine action: induced local unfolding of beta-tubulin, Biochemistry 32 (1993) 13560–13565, https://doi.org/10.1021/bi00212a023.
[11] A. Cormier, M. Knossow, C. Wang, B. Gigant, The binding of vinca domain agents to tubulin: structural and biochemical studies, Methods Cell Biol. 95 (2010) 373–390, https://doi.org/10.1016/s0091-679x(10)95020-6.
[12] P. Giannakakou, R. Gussio, E. Nogales, K.H. Downing, D. Zaharevitz, B. Bollbuck, G. Poy, D. Sackett, K.C. Nicolaou, T. Fojo, A common pharmacophore for epothilone and taxanes: molecular basis for drug resistance conferred by tubulin mutations in human cancer cells, Proc. Natl. Acad. Sci. U. S. A. 97 (2000) 2904–2909, https://doi.org/10.1073/pnas.040546297.
[13] C.C. Zhang, J.M. Yang, E. White, M. Murphy, A. Levine, W.N. Hait, The role of MAP4 expression in the sensitivity to paclitaxel and resistance to vinca alkaloids in p53 mutant cells, Oncogene 16 (1998) 1617–1624, https://doi.org/10.1038/sj.onc.1201658.
[14] E.C. McLoughlin, N.M. O'Boyle, Colchicine-binding site inhibitors from chemistry to clinic: a review, Pharmaceuticals 13 (2020), https://doi.org/10.3390/ph13010008.
[15] G. Nagaiah, S.C. Remick, Combretastatin A4 phosphate: a novel vascular disrupting agent, Future Oncol. 6 (2010) 1219–1228, https://doi.org/10.2217/fon.10.90.
[16] N. Koyanagi, T. Nagasu, F. Fujita, T. Watanabe, K. Tsukahara, Y. Funahashi, M. Fujita, T. Taguchi, H. Yoshino, K. Kitoh, In vivo tumor growth inhibition produced by a novel sulfonamide, E7010, against rodent and human tumors, Canc. Res. 54 (1994) 1702–1706.
[17] M.M. Mita, M.A. Spear, L.K. Yee, A.C. Mita, E.I. Heath, K.P. Papadopoulos, K.C. Federico, S.D. Reich, O. Romero, L. Malburg, M. Pilat, G.K. Lloyd, S.T. Neuteboom, G. Cropp, E. Ashton, P.M. LoRusso, Phase 1 first-in-human trial of the vascular disrupting agent plinabulin(NPI-2358) in patients with solid tumors or lymphomas, Clin. Canc. Res. 16 (2010) 5892–5899, https://doi.org/10.1158/1078-0432.Ccr-10-1096.
[18] E. Fox, Y.P. Mosse, H.M. Meany, J.G. Gurney, G. Khanna, H.A. Jackson, G. Gordon, S. Shusterman, J.R. Park, S.L. Cohn, P.C. Adamson, W.B. London, J.M. Maris, F.M. Balis, Time to disease progression in children with relapsed or refractory neuroblastoma treated with ABT-751: a report from the Children's Oncology Group (ANBL0621), Pediatr. Blood Canc. 61 (2014) 990–996, https://doi.org/10.1002/pbc.24900.
[19] T. Ma, A.D. Fuld, J.R. Rigas, A.E. Hagey, G.B. Gordon, E. Dmitrovsky, K.H. Dragnev, A phase I trial and in vitro studies combining ABT-751 with carboplatin in previously treated non-small cell lung cancer patients, Chemotherapy 58 (2012) 321–329, https://doi.org/10.1159/000343165.
[20] M.A. Rudek, A. Dasari, D. Laheru, P. He, R. Jin, R. Walker, G.E. Taylor, A. Jimeno, R.C. Donehower, M. Hidalgo, W.A. Messersmith, W.T. Purcell, Phase 1 study of ABT-751 in combination with CAPIRI (capecitabine and irinotecan) and bevacizumab in patients with advanced colorectal cancer, J. Clin. Pharmacol. 56 (2016) 966–973, https://doi.org/10.1002/jcph.681.
[21] T.J. Wang, H.T. Liu, Y.H. Lai, T.R. Jan, N. Nomura, H.W. Chang, C.C. Chou, Y.J. Lee, P.J. Tsai, Honokiol, a polyphenol natural compound, attenuates cisplatin-induced acute cytotoxicity in renal epithelial cells through cellular oxidative stress and Cytoskeleton modulations, Front. Pharmacol. 9 (2018) 357, https://doi.org/10.3389/fphar.2018.00357.
[22] H. Chen, S. Deng, Y. Wang, N. Albadari, G. Kumar, D. Ma, W. Li, S.W. White, D.D. Miller, W. Li, Structure-activity relationship study of novel 6-Aryl-2-benzoyl-pyridines as tubulin polymerization inhibitors with potent antiproliferative properties, J. Med. Chem. 63 (2020) 827–846, https://doi.org/10.1021/acs.jmedchem.9b01815.
[23] M.J. Lai, H.Y. Lee, H.Y. Chuang, L.H. Chang, A.C. Tsai, M.C. Chen, H.L. Huang, Y.W. Wu, C.M. Teng, S.L. Pan, Y.M. Liu, S. Mehndiratta, J.P. Liou, N-Sulfonylaminobiaryls as antitubulin agents and inhibitors of signal transducers and activators of transcription 3 (STAT3) signaling, J. Med. Chem. 58 (2015) 6549–6558, https://doi.org/10.1021/acs.jmedchem.5b00659.
[24] B. Shan, J.C. Medina, E. Santha, W.P. Frankmoelle, T.C. Chou, R.M. Learned, M.R. Narbut, D. Stott, P. Wu, J.C. Jaen, T. Rosen, P.B. Timmermans, H. Beckmann, Selective, covalent modification of beta-tubulin residue Cys-239 by T138067, an antitumor agent with in vivo efficacy against multidrug-resistant tumors, Proc. Natl. Acad. Sci. U. S. A. 96 (1999) 5686–5691, https://doi.org/10.1073/pnas.96.10.5686.
[25] A.L. Risinger, C.D. Westbrook, A. Encinas, M. Mülbaier, C.M. Schultes, S. Wawro, J.D. Lewis, B. Janssen, F.J. Giles, S.L. Mooberry, ELR510444, a novel microtubule disruptor with multiple mechanisms of action, J. Pharmacol. Exp. Therapeut. 336 (2011) 652–660, https://doi.org/10.1124/jpet.110.175331.
[26] N.A. Meanwell, Fluorine and fluorinated motifs in the design and application of bioisosteres for drug design, J. Med. Chem. 61 (2018) 5822–5880, https://doi.org/10.1021/acs.jmedchem.7b01788.
[27] R.F. Luduena, M.C. Roach, T.H. MacRae, G.M. Langford, N,N'-Ethylene-bis(iodoacetamide) as a probe for structural and functional characteristics of brine shrimp, squid, and bovine tubulins, Can. J. Biochem. Cell Biol. 63 (1985) 439–447, https://doi.org/10.1139/o85-063.
[28] K. Yoshimatsu, A. Yamaguchi, H. Yoshino, N. Koyanagi, K. Kitoh, Mechanism of action of E7010, an orally active sulfonamide antitumor agent: inhibition of mitosis by binding to the colchicine site of tubulin, Canc. Res. 57 (1997) 3208–3213.
[29] A. Dorléans, B. Gigant, R.B. Ravelli, P. Mailliet, V. Mikol, M. Knossow, Variations in the colchicine-binding domain provide insight into the structural switch of tubulin, Proc. Natl. Acad. Sci. U. S. A. 106 (2009) 13775–13779, https://doi.org/10.1073/pnas.0904223106.
[30] H. Harashima, N. Dissmeyer, A. Schnittger, Cell cycle control across the eukaryotic kingdom, Trends Cell Biol. 23 (2013) 345–356, https://doi.org/

10.1016/j.tcb.2013.03.002.
[31] G.R. Stark, W.R. Taylor, Control of the G2/M transition, Mol. Biotechnol. 32 (2006) 227–248, https://doi.org/10.1385/mb:32:3:227.
[32] C. Qi, X. Wang, Z. Shen, S. Chen, H. Yu, N. Williams, G. Wang, Anti-mitotic chemotherapeutics promote apoptosis through TL1A-activated death receptor 3 in cancer cells, Cell Res. 28 (2018) 544–555, https://doi.org/10.1038/s41422-018-0018-6.
[33] J.M. Adams, S. Cory, The Bcl-2 protein family: arbiters of cell survival, Science 281 (1998) 1322–1326, https://doi.org/10.1126/science.281.5381.1322.
[34] S.E. Logue, S.J. Martin, Caspase activation cascades in apoptosis, Biochem. Soc. Trans. 36 (2008) 1–9, https://doi.org/10.1042/bst0360001.
[35] J.E. Klaunig, Oxidative stress and cancer, Curr. Pharmaceut. Des. 24 (2018) 4771–4778, https://doi.org/10.2174/1381612825666190215121712.
[36] K. Sinha, J. Das, P.B. Pal, P.C. Sil, Oxidative stress: the mitochondria-dependent and mitochondria-independent pathways of apoptosis, Arch. Toxicol. 87 (2013) 1157–1180, https://doi.org/10.1007/s00204-013-1034-4.
[37] E. Porcù, A. Salvador, I. Primac, S. Mitola, R. Ronca, C. Ravelli, R. Bortolozzi, D. Vedaldi, R. Romagnoli, G. Basso, G. Viola, Vascular disrupting activity of combretastatin analogues, Vasc. Pharmacol. 83 (2016) 78–89, https://doi.org/10.1016/j.vph.2016.05.006.
[38] E.L. Schwartz, Antivascular actions of microtubule-binding drugs, Clin. Canc. Res. 15 (2009) 2594–2601, https://doi.org/10.1158/1078-0432.Ccr-08-2710.
[39] T. Sander, J. Freyss, M. von Korff, C. Rufener, DataWarrior: an open-source program for chemistry aware data visualization and analysis, J. Chem. Inf. Model. 55 (2015) 460–473, https://doi.org/10.1021/ci500588j.